Journal Pre-proof

Impact of a fresh-core mesoscale eddy in modulating oceanic response to a Madden-Julian Oscillation

M.V.C. Azaneu, Adrian J. Matthews, Karen J. Heywood, Rob A. Hall, Dariusz B. Baranowski

PII: S0967-0645(24)00040-7

DOI: https://doi.org/10.1016/j.dsr2.2024.105396

Reference: DSRII 105396

To appear in: *Deep-Sea Research Part II*

Received Date: 26 August 2023

Revised Date: 17 May 2024

Accepted Date: 8 June 2024

Highlights

Impact of a fresh-core mesoscale eddy in modulating oceanic response to a Madden-Julian Oscillation

M V. C. Azaneu, Adrian J. Matthews , Karen J. Heywood , Rob A. Hall , Dariusz B. Baranowski

- Ocean dynamics affect air-sea interaction via a lasting barrier layer induced by fresh-core mesoscale eddy.
- The presence of a thick eddy-induced BL modulates SST anomalies forced by surface fluxes during a typical MJO event.
- Suggests importance of mesoscale variability as an ocean dynamic component of the coupled MJO system that should be included in MJO modelling.

Impact of a fresh-core mesoscale eddy in modulating oceanic response to a Madden-Julian Oscillation

Dr M V. C. Azaneu[a,*], Adrian J. Matthews[b], Karen J. Heywood[a], Rob A. Hall[a] and Dariusz B. Baranowski[c]

[a]Centre for Ocean and Atmospheric Sciences, School of Environmental Sciences, University of East Anglia, Research Park, Norwich, NR4 7TJ, United Kingdom

[b]Centre for Ocean and Atmospheric Sciences, School of Environmental Sciences and School of Mathematics, University of East Anglia, Norwich, NR4 7TJ, United Kingdom

[c]Institute of Geophysics, Polish Academy of Sciences, Marcina Kasprzaka 44/52, Warsaw, 01-224, Poland

ARTICLE INFO

Keywords:
Eddies
Barrier layer
Air-sea interaction

ABSTRACT

Theories of ocean–atmosphere interaction during a Madden–Julian Oscillation (MJO) are generally based on a thermodynamic model with surface fluxes dictating changes in sea surface temperature. Evidence from a two month ocean glider deployment in early 2019 in the southeast Indian Ocean suggests the impact of mesoscale dynamics on upper-ocean stratification likely affects ocean–atmosphere interaction at MJO scales. Until mid-February, local surface fluxes consistent with a convectively suppressed MJO phase drove near-surface ocean evolution. With the advection of a fresh-core eddy to the glider location in late February, ocean dynamics then becomes an additional driver of this evolution by modulating local stratification and generating a barrier layer of ≈12 m thickness for 10 days. One-dimensional modelling experiments based on the ocean and atmospheric conditions experienced during our sampling period show that the ocean subsurface structure within the eddy induce changes in SST of physical significance for ocean-atmosphere interaction. Moreover, results also suggest that the presence of a thick eddy-induced barrier layer during the MJO suppressed phase modulates the magnitude of temperature anomalies forced by surface fluxes during the following enhanced MJO phase. As eddies are abundant in this area, their dynamics must be considered to correctly represent SST variability for MJO modelling.

1. Introduction

The Madden–Julian Oscillation (MJO) is the dominant mode of intraseasonal variability in the tropical atmosphere (Zhang, 2005). It is a primary driver of extreme precipitation over the Maritime Continent (Da Silva and Matthews, 2021), and impacts weather regimes as far away as western Europe (Cassou, 2008). Notwithstanding, the MJO remains a major source of predictability in medium-range global weather forecasting (Lin, Brunet and Fontecilla, 2010). Ocean–atmosphere coupling is an important component within the MJO (DeMott, Klingaman and Woolnough, 2015) and is a major challenge in improving MJO prediction (Jiang, Adames, Kim, Maloney, Lin, Kim, Zhang, DeMott and Klingaman, 2020). The primary ocean–atmosphere coupling mechanism is thermodynamic: fluctuations in shortwave radiation and latent heat fluxes lead to changes in ocean mixed layer temperature, and surface temperature changes feed back onto atmospheric convection (Shinoda, Hendon and Glick, 1998). Basin-wide ocean dynamics in the form of oceanic equatorial Kelvin and Rossby waves also change sea surface temperatures (SSTs) through upwelling and downwelling (Webber, Matthews and Heywood, 2010). Here, we present evidence that a third component of ocean–atmosphere coupling is also important in MJO development, namely the action of mesoscale eddies.

In the southeast tropical Indian Ocean (SETIO), the flow is highly energetic at intraseasonal (40–80 days) time scales, due to the confluence of several currents and generation of meanders and eddies from their instability (Feng and Wijffels, 2002; Wang, Cheng, Liu and Chen, 2021). These eddies are sufficiently long lived (50 ± 22 and 53 ± 25 days, respectively; Wang et al., 2021) to impact the transport of heat and salt in the southern branch of the subtropical gyre (Feng and Wijffels, 2002)

Besides the direct impact on SST due to the heat transport, the transport of salt by these eddies may also have an impact on SST by affecting the hydrographic structure of the ocean near surface. Then advection of relatively fresh waters, for example from the Indonesian Throughflow (Bray, Wijffels, Chong, Fieux, Hautala, Meyers and Morawitz, 1997), can form fresh water lenses at the surface which, depending on the temperature structure, can form a so called "barrier" layer (BL; Godfrey and Lindstrom, 1989).

Several studies have investigated the role of BLs in affecting air-sea interaction through changes on SST at different scales. For example, Balaguru, Foltz, Ruby Leung, Kaplan, Xu, Reul and Chapron (2020) shows the important role of salinity in tropical cyclones rapid intensification in the eastern Caribbean Sea and the western tropical Atlantic. In the western Pacific warm pool, it has been suggested that the BL helps buildup heat during El Niño events (Maes, Picaut and Belamari, 2005) and may play an active role

*Corresponding author
thumbnails/cas-email.jpeg m.azaneu@uea.ac.uk (M.V.C. Azaneu)
ORCID(s): 0000-0002-7538-3056 (M.V.C. Azaneu)

in ENSO evolution (Zhu, Huang, Zhang, Hu, Kumar, Balmaseda, Marx and Kinter, 2014). Using composited observations, Drushka, Sprintall and Gille (2014) shows that the upper ocean temperature response to MJO forcing is reduced in the presence of a thick BL in the eastern equatorial Indian Ocean. They did not find, however, a strong signal of the MJO on the BL thickness, which was attributed to the variability of individual MJO events. The difference in the ocean response to this variability in MJO events is still to be considered. Modelling studies have also explored the sea surface salinity feedback to the MJO, which was suggested to be negligible (Zhu and Kumar, 2019). However, limitations on the model representation of BL were pointed out as possibly biasing these results and thus the BL impact on MJO and its predictability cannot be dismissed.

As SST is particularly high in the SETIO region, even small variations can lead to large changes in atmospheric convection (Gadgil, Joseph and Joshi, 1984). Therefore, the ubiquitous mesoscale variability in this region has the potential to impact air–sea interactions and coupled weather systems such as the MJO. In this study we focus on the role that mesoscale eddies have in generating BLs, and its potential to induce changes in SST. Using high resolution data from ocean gliders, we present in situ evidence and runs from 1-D model suggesting that mesoscale dynamic variability is capable of impacting the upper ocean stratification sufficiently to be relevant for ocean–atmosphere interaction in the MJO. We highlight mesoscale variability as a dynamic component of the coupled MJO system in the Indian Ocean.

2. Glider data and methods

Two Seagliders (SG537 and SG641) were deployed in the SETIO between Christmas Island and the Java coast (Fig. 1), sampling the ocean upper 1000 m as virtual moorings (within ~ 2 km of the target location) between 30 January and 15 March 2019 (Fig. 2). Profiles of conservative temperature (Θ) and absolute salinity (S; both vertical resolution $0.1-0.5$ m) were smoothed with a 2.5 m running median filter, and then vertically averaged onto a regular 1-m depth grid to produce surface time series (averaged between 0-30 m; Θ_g and S_g respectively).

Isothermal layer depth (m; ILD) and mixed layer depth (m; MLD) were calculated using differences of temperature, salinity and potential density from a reference depth (D) of 3 m ($\Theta_{ref} = \Theta_{D=3}$, $S_{ref} = S_{D=3}$ and $\sigma_{ref} = \sigma_{D=3}$, respectively). ILD was defined as the depth at which temperature decreases to $\Delta\Theta = 0.3$°C below Θ_{ref} (Sprintall and Tomczak, 1992; Drushka et al., 2014):

$$\text{ILD} = D|_{\Theta=\Theta_{ref}-\Delta\Theta} . \tag{1}$$

MLD was calculated as:

$$\text{MLD} = D|_{\sigma_\theta=\sigma_{ref}+\Delta\sigma_\theta} , \tag{2}$$

where $\Delta\sigma_\theta$ is the change in potential density equivalent to $\Delta\Theta$, assuming S is constant:

$$\Delta\sigma_\theta = \sigma_\theta(\Theta_{ref}-\Delta\Theta, S_{ref}, P_0) - \sigma_\theta(\Theta_{ref}, S_{ref}, P_0). \tag{3}$$

Here, P_0 is pressure at the ocean surface.

Where near-surface stratification is dominated by salinity, MLD can be shallower than ILD, forming a barrier layer (BL) of homogeneous temperature. Here, we define barrier layer thickness (BLT) as ILD minus MLD. Near-surface stratification is quantified as a potential energy anomaly (ϕ; J m^{-3}), integrated from the surface to a depth (H) of 350 m:

$$\phi = \frac{1}{H}\int_{-H}^{0}[\overline{\sigma} - \sigma(z)]gz\,dz . \tag{4}$$

where $\overline{\sigma}$ is vertical-mean density over same depth range. Extending the integration below 350 m did not significantly change estimates of ϕ, indicating that most eddy variability is above this depth. This agrees with Yang, Yu, Yuan, Zhao, Wang, Chen, Liu and Duan (2015), who showed that eddy temperature and salinity anomalies were confined to the upper 300 m. In section 7, we assess the stratification strength of the surface layer from daily-averaged glider profiles. For these, we integrate ϕ from the surface to a depth (H) of 40 m (ϕ_{40}), chosen due to representing the deepest ILD among the profiles considered. Positive ϕ indicates static stability, being the amount of energy required to vertically mix the water column down to H. Positive $\partial\phi/\partial t$ (potential energy anomaly tendency) indicates a source of stratification; negative $\partial\phi/\partial t$ indicates a sink of stratification.

Here, steric height anomaly (δ) is dynamic height anomaly divided by global-average gravitational acceleration (IOC, SCOR and IAPSO, 2010) with a 350 m level of no motion. MJO phase is defined by the real time multivariate MJO (RMM) index (http://www.bom.gov.au/climate/mjo/; Wheeler and Hendon, 2004).

3. Atmospheric variability

The high-resolution glider virtual mooring data coincided with a transition between MJO events. The first month occurred during a suppressed convective phase of the MJO (hereafter *suppressed phase*) and thus dry conditions over the SETIO (red bars in Figs. 2 and 3). This was followed by two weeks of a MJO enhanced convective phase (hereafter *enhanced phase*) and thus wet conditions (dark blue bar). Here, we show that during this period local thermodynamic forcing at the glider location was consistent with a canonical MJO.

During the suppressed phase (red bar in Fig. 3), ERA5 reanalysis (Hersbach, Bell, Berrisford, Hirahara, Horányi, Muñoz-Sabater, Nicolas, Peubey, Radu, Schepers, Simmons, Soci, Abdalla, Abellan, Balsamo, Bechtold, Biavati, Bidlot, Bonavita, De Chiara, Dahlgren, Dee, Diamantakis, Dragani, Flemming, Forbes, Fuentes, Geer, Haimberger, Healy, Hogan, Holm, Janisková, Keeley, Laloyaux, Lopez, Lupu, Radnoti, de Rosnay, Rozum, Vamborg, Villaume and Thépaut, 2020) average net surface heat flux, defined as a sum of surface sensible heat flux, latent heat flux, shortwave radiation flux and longwave radiation flux (hereafer heat flux), at the location of glider SG537 was 99 W m^{-2}, indicating ocean gaining heat from the atmosphere (Fig. 3a). ERA5 net fresh water flux was mostly negative (average $-0.1\,\mathrm{mm\,d^{-1}}$; Fig. 3a), as precipitation was very low or absent whereas evaporation was fairly constant (Fig. 3b).

In the transition to the enhanced convection phase (blue bar in Fig. 3), the net heat flux decreased and approached zero (average $-1\,\mathrm{W\,m^{-2}}$; Fig. 3a). Precipitation increased both in ERA5 and in the independent TRMM 3B42 Multi-Satellite Precipitation Analysis TMPA (Kummerow, Simpson, Thiele, Barnes, Chang, Stocker, Adler, Hou, Kakar, Wentz, Ashcroft, Kozu, Hong, Okamoto, Iguchi, Kuroiwa, Im, Haddad, Huffman, Ferrier, Olson, Zipser, Smith, Wilheit, North, Krishnamurti and Nakamura, 2000). As a result, the net fresh water flux was on average positive in this period (average $12.5\,\mathrm{mm\,d^{-1}}$; Fig. 3a). Although ERA5 surface wind speed did not change significantly between the suppressed and enhanced phases (from $4.1\,\mathrm{m\,s^{-1}}$ to $4.2\,\mathrm{m\,s^{-1}}$), the large scale wind field changed from easterly to westerly (not shown).

These observed changes in ERA5 winds, heat and fresh water fluxes at the glider location are thermodynamically consistent with the evolution of a typical MJO event in the region. Thus, we conclude that the large-scale MJO-associated physical processes are realised at the local scale (i.e. at the glider location) and that our observations occurred during a typical, well-characterised canonical MJO.

4. Drivers of ocean mixed layer variability

The heat and salt fluxes associated with the evolution of the MJO discussed in section 3 (Fig. 3a,b) will influence the temperature and salinity of the upper ocean. To assess this influence at the glider location, we first test the hypothesis that the surface ocean temperature and salinity evolution is controlled thermodynamically by the local MJO-related surface fluxes only, with dynamics and the contribution from vertical mixing and entrainment having a negligible role. To that end, we create a simple model which assumes that surface fluxes are absorbed and instantly redistributed within the ML (an equivalent of a slab ocean model) and they are the sole contributor to changes in upper ocean temperature and salinity.

If the ERA5 net heat flux Q were the only source of temperature change in the surface ocean, and if that heat were distributed over a mixed layer of depth h, then the theoretical thermodynamically-forced temperature tendency is:

$$\frac{\partial \Theta_t}{\partial t} = \frac{Q}{\rho_w c_p h}\,, \tag{5}$$

where $\rho_w = 1021\,\mathrm{kg\,m^{-3}}$ is the mixed layer density and $c_p = 3991\,\mathrm{J\,kg^{-1}\,K^{-1}}$ is the specific heat capacity of seawater. A theoretical temperature (Θ_t) time series is estimated by integrating Equation 5 with respect to time and using the glider observations (Θ_g; Fig. 3d) to constrain the integration constant. A value of $h = 30$ m, which corresponds approximately to the deepest observed MLD (Fig. 3e), was found to give the best fit to the observed temperature time series.

Similarly, a theoretical salinity (S_t) time series forced by the surface freshwater flux is calculated by integrating the following equation with respect to time:

$$\frac{\partial S_t}{\partial t} = -\frac{F\bar{S}_g}{\sigma_w h}\,, \tag{6}$$

where F is the net surface freshwater mass flux (Damerell, Heywood, Thompson, Binetti and Kaiser, 2016).

As expected from the positive (downward) net surface heat flux during the suppressed phase (Fig. 3a), Θ_t exhibits a persistent increasing trend which is closely tracked by the observed Θ_g for the majority of this period (Fig. 3d). Similarly, S_t and S_g agree and do not vary greatly until the second half of the suppressed phase (Fig. 3c). This indicates that, during this period, the surface ocean temperature and salinity tendencies can be accounted for solely by the net heat and freshwater fluxes in this period. Therefore vertical entrainment from below the mixed layer and horizontal advection make negligible contributions to the surface budgets.

However, from late February, both Θ_g and S_g diverge from Θ_t (Fig. 3d) and S_t (Fig. 3c), respectively. This indicates that the temperature and salinity tendencies cannot be accounted for by net surface fluxes, and therefore other ocean processes must be important. The beginning of the divergence between S_g and S_t is clearly marked by an abrupt decrease in surface salinity from 34.6 to $33.9\,\mathrm{g\,kg^{-1}}$ on 18 February (Fig. 3c). This coincided with a sharp increase in steric height anomaly (δ), which reached its peak (∼1.19 m) on 24 February (Fig. 3f). These distinct variations in S_g and δ lasted for approximately 10 days (until 28 February). Together with a simultaneous depression of the subsurface isotherms (Fig. 2), this suggests the passage of a fresh-core mesoscale anticyclonic eddy.

The eddy signature in surface temperature (Fig. 3d) is not as evident as it is in salinity (Fig. 3c), since there is no marked divergence between Θ_g and Θ_t. However, coincident with the sharp decrease in observed S_g, Θ_g increases by 0.61 °C (from 29.07 °C to 29.68 °C) between 18-22 February, which is twice the increase in Θ_t (0.30 °C, from 29.23 °C to 29.53 °C). Thus, the eddy makes a direct advective contribution to the increase in temperature locally, although it is secondary to the thermodynamic warming from surface fluxes during the suppressed phase. The stronger eddy effect in salinity is in agreement with Li and Wang (2015), who show in model runs of this region that ocean internal processes account for a greater percentage of sea surface salinity intraseasonal variability (10 %) than for temperature (less than 5 %), for which vertical processes are highly important.

Similar features are also observed at the location of glider SG641 (not shown), where changes in salinity and δ are observed after 23 February, five days after they are observed by SG537. SG641 was approximately 100 km southwest of SG537 (Fig. 1). This confirms the persistence of the eddy signature and indicates an eddy speed of translation of approximately $0.23\,\mathrm{m\,s^{-1}}$. This speed of translation is the same order of magnitude as altimetry-based estimates of the mean zonal speed of anticyclonic eddies ($0.16\,\mathrm{m\,s^{-1}}$) in the SETIO region (Yang et al., 2015).

The eddy then leaves the location of SG537 around 28 February, marked by a decrease in δ after the peak on 24 February (Fig. 3f) and an increase in S_g (Fig. 3c). Immediately after, the net freshwater flux becomes positive (Fig. 3f) due to the increase in precipitation during the enhanced phase (Fig. 3b), which leads to a subtle steady decrease in S_t until late March (Fig. 3c). This is broadly followed by S_g (Fig. 3c). However, the S_g tendency is highly variable through this period, in contrast to the nearly constant S_t tendency, indicating freshwater contribution from other sources besides the surface flux.

Our analysis indicates that for the majority of the suppressed phase, the surface ocean variability is primarily driven thermodynamically by the surface fluxes. However, from late February, ocean dynamics become an important driver of variability due to the advection of a fresh-core eddy.

5. Eddy evolution from ocean reanalysis

The observations in Section 4 have provided compelling evidence of the presence of an anticylonic eddy and its effect on the local salinity and temperature tendencies. In this section, we use the greater spatio-temporal coverage of the CMEMS global ocean eddy-resolving reanalysis product GLORYS12V1 (1/12° horizontal resolution; Lellouche, Eric, Romain, Gilles, Angélique, Marie, Clément, Mathieu, Olivier, Charly, Tony, Charles-Emmanuel, Florent, Giovanni, Mounir, Yann and Pierre-Yves, 2021) to provide a more detailed analysis of the eddy properties and evolution.

Using GLORYS12V1 temperature and salinity surface maps, the eddy origin was traced back to a South Java Current (SJC) retroflection around 9°S, 110°E in late January (Fig. 4a), with contribution from low salinity waters from Sunda Strait once the eddy is formed (approximately 9°S, 109°E; Fig. 4b). As the eddy evolved, it was advected westward as a coherent vortex and reached the SG537 glider location (18 February; Fig. 4c,d) as seen in salinity and δ (Fig. 3c,f). GLORYS12V1 also indicates the presence of low-salinity eddy-transported waters at the glider location at least until 4 March. Between 28 February and 4 March (Fig. 4e,f), however, the eddy signature is not distinctive in δ (Fig. 3f) as it is no longer a coherent vortex, but rather an eddy-filament system. Thus, even after the eddy is no longer detectable in δ, the waters advected within it still affect the variability of near-surface hydrography for several days and consequently contribute to the differences between S_g and S_t tendencies (Fig. 3c). After 4 March, an outflow of low salinity waters from Sunda strait reaches the glider, strongly attenuating the local contribution of the eddy-transported waters (not shown).

6. Impact of eddy advection on ocean stability

The eddy advection by the mean current changes the vertical temperature and salinity distribution and therefore stratification at the glider location. This can be diagnosed from $\partial\phi/\partial t$ as the eddy passes the glider location (Fig. 3f). As the eddy approaches, $\partial\phi/\partial t$ becomes positive, indicating an increase in stratification with time. The eddy centre (maximum δ) coincides with $\partial\phi/\partial t$ becoming negative (a decrease in stratification with time), which persists until the eddy has passed. Therefore, the eddy was a source of local potential energy and stratification.

The relative contribution of vertical temperature and salinity gradients to the upper ocean stability is expressed as Turner angle values (Tu; Fig. 3g; Ruddick, 1983). Mixed layer Tu indicates a change from a regime mostly prone to salt-fingering ($45° < Tu < 90°$), in which salinity has a destabilising effect, to a regime in which waters above the ILD are predominantly stably stratified in both temperature and salinity ($-45° < Tu < 45°$) during advection of the eddy. This is consistent with the change from warm and salty conditions associated with the suppressed phase surface fluxes, to warm and fresh conditions due to the influence of eddy-transported waters. This increase in the stability of the water column is in agreement with positive $\partial\phi/\partial t$ (Fig. 3f).

Afterwards, with the enhanced phase characteristic increase in precipitation and heat loss to the atmosphere, the ML waters become diffusively unstable, i.e., temperature has a destabilising effect ($-90° < Tu < -45°$). Nevertheless, waters within the BL remain stably stratified, evidencing the efficiency of the BL in isolating the ML from deeper waters. Thus, even though both the fresh-core eddy and enhanced precipitation can lead to BL formation, the stability of the water column is highest when only the eddy is present, as there is an input of fresh waters without heat loss. This suggests that the eddy effect on ocean stability likely produces a stronger barrier to wind mixing than that arising from precipitation. Identifying this change in static stability regime induced by the eddy is only possible due to the high-resolution in situ observations; general circulation models would not be able to capture this process.

Due to the eddy-transported fresh-waters (Fig. 2) and consequent increase in stratification and stability (from 18-02-2019; Fig. 3f,g), the MLD shoals (Fig. 2 and Fig. 3e). However, the ILD does not shoal (Fig. 2) and consequently a 12 m thick BL is formed (18-02-2019 to 24-02-2019; Figs. 2 and 3e). The BL was absent before the arrival of the eddy (before 18-02-2019; Fig. 3e), as the MLD and ILD coincided (Fig. 2). This is consistent with ML stratification controlled by heat flux and thus ocean temperature. The eddy arrived during the suppressed phase (Fig. 3), i.e., net fresh water flux was near-zero (Fig. 3a). Thus, surface fluxes did not contribute to generating the BL, whose initial formation was solely due to the eddy.

Conversely, the effect of the eddy-filament system on the ocean stratification acted to maintain the BL after its initialization (Fig. 3e). Within the period of influence of the eddy/eddy-filament system, the BLT varied between 12–20 m, being thickest during the enhanced phase, associated with periods of enhanced precipitation (Fig. 3b). Thus, while the eddy initiated the BL of $\sim$ 12 m, the precipitation associated with the enhanced phase acted to thicken it.

The BL initiation by the eddy in the suppressed phase potentially influenced the surface ocean behaviour during the enhanced phase. The upper ocean response to the MJO is sensitive to the atmospheric forcing itself and to the upper ocean stratification (Drushka et al., 2014). For example, a strong ML freshening occurring before the onset of the enhanced phase could counteract MJO-induced wind mixing, leading to a MLD that remains shallow and to the BL development if the temperature stratification is weak. Thus, the increase in stratification and BL initiation by the eddy during the suppressed phase likely modulate the ocean response during the enhanced phase, supporting further development of the BL induced by the atmospheric system.

The existence of a BL can affect SST in several ways, for example by reducing entrainment of cooler water at the base of the ML and by constraining wind-induced momentum within the ML (Godfrey and Lindstrom, 1989; Vialard and Delecluse, 1998). Incoming shortwave heat flux is restricted within the shallower ML rather than being distributed throughout the IL. Thus, mixed layer heat capacity is reduced, leading to a greater SST response to a given heat flux in comparison with a deeper ML (Drushka et al., 2014; DeMott, Benedict, Klingaman, Woolnough and Randall, 2016). We estimate the theoretical effect of the eddy-induced BL on SST ($\partial\Theta_t/\partial t$) by changing the thickness of the layer through which the heat flux will be distributed in Eq. 5.

After the arrival of the eddy in late February, the surface heat flux was $Q \approx 100\,\mathrm{W\,m^{-2}}$ (Fig. 3a) and the ILD was $h \approx 30\,\mathrm{m}$ (Fig. 2). In the absence of a barrier layer, this heat flux would be distributed through the full IL, leading to $\partial\Theta_t/\partial t \approx 0.07\,°\mathrm{C\,d^{-1}}$. In our observation, the eddy-induced BL ($\sim$10 m thickness) (Fig. 3e) reduced the MLD to $h \approx 20\,\mathrm{m}$, increasing $\partial\Theta_t/\partial t$ to $\approx 0.11\,°\mathrm{C\,d^{-1}}$. Hence, the potential extra warming due to the eddy-induced BL constraining the heating to a shallower ML is the difference between these two values: $0.04\,°\mathrm{C\,d^{-1}}$.

The eddy-induced BL lasted for $\sim$10 days. This is comparable to the time scale that the MJO changes from a neutral to a convectively active phase at a given location (i.e., a quarter of the approximately 45-day MJO). Hence, the potential extra warming induced by the BL over this period is $\partial\Theta_t/\partial t \approx 0.4\,°\mathrm{C}\,(10\,\mathrm{day})^{-1}$. A warming of this magnitude, over this time scale, is physically relevant in the ocean–atmosphere interactions associated with the MJO, and thus merits further investigation.

In our effective Eulerian framework (i.e., at "fixed" glider location), we would not expect to directly observe this extra warming because of the relatively long time required for the localized thermodynamic effect of the BL to take effect, in this case 0.4 °C over 10 days. The horizontal length scale of the eddy is approximately 100 km (Fig. 4) and its speed of translation is $c \approx 20\,\mathrm{km\,d^{-1}}$, leading to an advective time scale of order 5 days. Hence, a parcel of water subject to the potential extra warming due to the BL would be advected away from the glider before this warming could be realised. In order to directly infer the effect of these changes, it would be necessary to either carry out a Lagrangian observational study with gliders following a specific eddy, or to perform a targeted modelling experiment. Here, we run one-dimensional modelling experiments using the Price-Weller-Pinkel (PWP) bulk mixed layer model (Price, Weller and Pinkel, 1986), where changes in ocean heat content are driven not only by surface heat fluxes but also by vertical mixing and entrainment.

7. PWP model experiments

7.1. Model setup

The PWP mixed layer model is used to evaluate the effect of a barrier layer in the evolution of the ML properties under different atmospheric forcing scenarios. The model is forced with wind stress and surface heat, radioative and moisture fluxes, and uses a dynamic instability criteria (bulk and gradient Richardson numbers) to mix based on vertical density gradients and current shear. Despite being a relatively simple model, many studies have demonstrated the skill of PWP in modelling deepening of mixed layers induced by winds (e.g. Plueddemann and Farrar, 2006; Baranowski, Flatau, Chen and Black, 2014; Damerell, Heywood, Calvert, Grant, Bell and Belcher, 2020; Alford, 2020).

We run 3 sets of experiments, each one being forced with hourly ERA-5 parameters representing different MJO conditions experienced during the glider deployment (Table 1). For experiment "MJOsup", winds, heat and fresh water fluxes are based on the conditions experienced between 10-02-2019 to 20-02-2019 and represent conditions under a suppressed MJO phase (Fig. 5). For experiment "MJOen", the forcing parameters are based on the period between 03-03-2019 to 13-03-2019 and represent conditions under an enhanced MJO phase. The third experiment ("MJOenW") represents conditions under an enhanced MJO but with stronger winds. For that, we use wind stress and latent heat flux from 18-01-2019 to 28-01-2019, and all remaining parameters from the same period as experiment MJOen (03-03-2019 to 13-03-2019). We set all forcing parameters as a constant average value for each defined period, except for short wave radiation, for which the average daily cycle is used. The model runs are output hourly and run for 10 days (e.g. Fig. 6), which represents the period that the BL lasted in our observations as estimated in Section 6.

For each experiment, there are 4 runs (Table 2), from which one is initialised with observed temperature and salinity from the glider location just before the arrival of the eddy, representing ocean conditions where the BL is absent (day 13-02-2019: run "NOEDDY"). The remaining runs were initialised with consecutive profiles from inside the eddy, representing conditions where the BL is present (days 19-02-2019: run "EDDYa"; 20-02-2019: run "EDDYb"; 21-02-2019: run "EDDYc"). We estimate the impact of the BL in the SST by comparing the simulated temperature time series from each of the EDDY runs with the NOEDDY run, which represents a "control run" (Fig. 7).

The days used to initialise the EDDY runs (EDDYa, EDDYb and EDDYc) represent different ocean conditions, as their temperature, salinity and density profiles have distinct stratification strength, MLD and BLT (Table 2 and Fig. 8). Profiles from day 19-02-2019 (run EDDYa) and day 21-02-2019 (run EDDYc) have similar BLT (7 m and 10 m, respectively) but very different MLD (10 m and 27 m, respectively; Fig. 8b,d). Day 20-02-2019 (run EDDYb; Fig. 8c) has a thicker BL (18 m) and intermediate MLD (15 m). The profile used to initialize the NOEDDY run (day 13-02-2019; Fig. 8a) has no BL and a MLD (25 m) similar to the MLD from the profile used for run EDDYc (Fig. 8d). Among profiles used for the EDDY runs, the stratification strength in the top 40 m (ϕ_{40}) decreases gradually from day 19-02-2019 to 21-02-2019 (Table 2). Profile from day 20-02-2019 (run EDDYb; Fig. 8c) has similar stratification strength as day 13-02-2019 (run NOEDDY), which is primarily induced by salinity in the former and temperature in the latter.

We calculate offline the contributions to stratification from net heat flux (Q) and wind speed (w), to gain insights into the dominant mechanisms acting to change the ocean stratification in each experiment. The rate of change of ϕ with time due to wind mixing $(\frac{\partial \phi}{\partial t})_w$ (W m^{-3}) is estimated as:

$$(\frac{\partial \phi}{\partial t})_w = -e_s k_s \rho_a (\frac{w^3}{H}) \tag{7}$$

where H is water depth (40 m, as in ϕ_{40}), k_s is the surface drag coefficient (2.4 x 10^{-5}), e_s is the fraction of turbulent energy produced at the surface that is available to work against stratification (0.023) and ρ_{air} is the density of air (typically 1.2 kg m^{-3}). The rate of change of ϕ with time due to surface fluxes $(\frac{\partial \phi}{\partial t})_Q$ (W m^{-3}) is estimated as:

$$(\frac{\partial \phi}{\partial t})_Q = \frac{\alpha g Q}{2 c_p} \tag{8}$$

where α is the thermal expansion coefficient (1.6×10^{-4}°C^{-}1) and c_p is the specific heat capacity of seawater (3991 J kg^{-1} K^{-1}), following Simpson and Sharples (2012).

7.2. Experiment MJOsup: suppressed MJO forcing

In the MJO suppressed phase experienced during our observations, heat fluxes are intense, while wind anomalies are weak (Fig. 5). Consistent with this, in the MJOsup experiment, $(\frac{\partial \phi}{\partial t})_Q$ (integrated for the 10 days of run = 20 J m^{-3}) is the main factor leading to changes in ϕ and contributing to its increase, as $(\frac{\partial \phi}{\partial t})_w$ is comparatively negligible (integrated for the 10 days of run = -0.6 J m^{-3}). As a consequence, for all runs ϕ, e.i. stratification, increased by the end of the runs (not shown).

In this experiment, the near-surface ocean (above 40 m) warms up at similar rates for all runs, regardless of the stratification strength of the water column and the presence of a BL (Figs. 7a). The model produces ILD and MLD that become shallower or have minimal changes, reaching daily average values between 9–15 m in the last day of the runs (Figs. 7a,b and 8). The existing BL in the profiles used to initialise the EDDY runs disappears in all runs, as ILD gets very shallow due to surface warming, which then defines the MLD (e.g. Figs. 6a, 7c and 8b,c,d). In all runs, warming is intensified in the top 10-15 m, showing a SST increase of 0.8–1.1 °C (Fig. 8, and Fig. 9a). In the EDDY runs, SST increases by 0.15–0.25 °C more than in the NOEDDY run (Fig. 9b,c,d).

Thus, the results show that, under the forcing of the suppressed MJO experienced during our observations (MJOsup, Fig. 5), the near-surface ocean behaves in a similar way regardless of the existence of a BL. The surface layer warms considerably, particularly in the top 10 m, leading to shallowing of the IL and ML, and the disappearance of a BL, if present initially (Figs. 7 and 8). The SST warming (0.8–1.1 °C) is in agreement with the positive net heat flux and low wind stress characteristic of the suppressed MJO phase, and it is 0.15–0.25 °C greater when the BL was initially present (Fig. 9b,c,d). This greater warming can be explained by the effect of the BL in reducing turbulent mixing and cooling at the base of the ML. As the BL got thinner but was still present for most of the run, it likely reduced cooling at depth and led to a greater warming compared with the run where the BL was absent.

7.3. Experiment MJOen: enhanced MJO forcing

The enhanced MJO phase experienced during our observations (and used as forcing for experiment MJOen) showed the expected negative heat fluxes and positive fresh water fluxes, but not a particularly strong wind stress (Fig. 5). As a consequence, in the MJOen experiment, integrated $(\frac{\partial \phi}{\partial t})_Q$ and $(\frac{\partial \phi}{\partial t})_w$ make similar contribution (∼-1 J m^{-3}) to changes in ϕ, which decreases during the run (not shown).

For all runs, MLD has minimal changes during the runs (< 5 m; Figs. 7 and 10). Waters in the ML freshen and cool (by 0.3-0.5 °C), leading to a deeper ILD (e.g. Figs. 6b and 10). In the NOEDDY run, waters in the top 25 m freshen and cool, with surface intensification (Figs. 10a and 11a). There is barely any change in the MLD during this run, while the ILD deepens slightly (5 m), forming a 5 m BL by the end of the run (Figs. 7b and 10a).

For the EDDY runs, in both EDDYa and EDDYb runs the ILD deepens strongly (by ∼ 28 m), increasing the BL considerably (BLT ∼ 30 m; e.g. Figs. 7c, 6b and 10b,c). In contrast, in the EDDYc run, neither MLD and ILD deepening is prominent (4–5 m), leading to a BL at the end of the run that is deeper, but of same thickness (∼ 10 m) as in its initial conditions (Figs. 7c and 10d). The strongest cooling (by 0.5 °C for SST) and biggest change in ILD occur for the run that was initialized with the profile with the shallowest MLD (day 19-02-2019; run EDDYa; Fig. 10b), which is 0.12°C colder than SST changes observed in the NOEDDY run (Fig. 11b). By contrast, the least cooling (by 0.5 °C for SST) occurs for the run with the deepest MLD (day 21-02-2019; run EDDYc; Fig. 10d), which represents less cooling than the NOEDDY run by 0.15 °C for SST (i.e., warmer; Fig. 11d).

The minimal changes in the MLD during the MJOen runs (e.g. Figs. 7b, 6b and 10 and) suggest that the surface forcing was not sufficiently strong to counteract the existing stratification and mix below the ML. This is in agreement with the forcing used in this experiment, in which wind stress was not particularly strong. In this way, waters above the ML freshen and cool (0.3–0.5 °C; Fig. 10) due to the negative heat flux and positive freshwater flux. As surface waters cool, ILD deepens, while fresher waters remain trapped above the ML. As a result, a BL is formed if absent (Fig. 10a), and it thickens if it already exists (Fig. 10b,c,d), isolating even more the surface waters from waters below.

The difference in the amount of cooling experienced in each run suggests that, due to the subsurface barrier created by the development/thickening of the BL in all runs, the amount of cooling the near-surface waters undergo is dictated by the ML heat capacity and the stratification strength of the initial profile. For example, the profile used to initialize run EDDYa (Fig. 10b) has a ML that is shallower than the ML from the NOEDDY run initial profile (Fig. 10a), and thus it undergoes stronger cooling by the end of the run due to the lower ML heat capacity (Fig. 11b). Similarly, the initial profile for run EDDYc shows less cooling (Fig. 10d) as ML is deeper in its initial profile (Fig. 11d). Thus, under these conditions of relatively weak winds, the presence of the BL in the initial profile was not the most important factor defining the amount of cooling of surface waters, but rather the MLD defining the heat capacity of the surface ocean. However, the development (NOEDDY run), maintenance (EDDYc run) and thickening (EDDYa,b runs) of the BL that was feasible under these atmospheric conditions likely contributed to isolating the surface waters and reducing subsurface cooling through the run.

7.4. Experiment MJOenW: enhanced MJO forcing with stronger winds

In experiment MJOenW, the forcing represents an enhanced MJO condition, with winds stronger than in MJOen. As a result, integrated $(\frac{\partial \phi}{\partial t})_Q$ (~-3.8 J m^{-3}) and $(\frac{\partial \phi}{\partial t})_w$ (~-5.8 J m^{-3}) is more negative than in experiment MJOen, leading to a greater overall decrease in ϕ, with a greater contribution from the wind energy input.

Similarly to what is observed in the MJOen experiment, in experiment MJOenW waters on the top 25 m freshen and cool in the NOEDDY run (Figs. 7a, 10a and 12a), with stronger anomalies in the MJOenW experiment. The ILD and MLD deepening is not prominent (~ 5 m) and are coincident, leading to the absence of a BL in the MJOenW-NOEDDY run (Figs. 7c and 12a).

For the MJOenW-EDDY runs, waters on the top 20–35 m freshen and cool by similar amounts to MJOen runs (e.g. Figs. 7a, 6c and 12b,c,d). In both MJOenW-EDDYa and MJOenW-EDDYb runs, the ILD deepens to similar depths as in experiment MJOen (Figs. 6b,c, 10b,c, 12b,c). Unlike experiment MJOen, in MJOenW experiment the MLD deepens (by 5–15 m) during the run (Figs.7b and 12b,c). As a consequence, the BLT increases, but less than in experiment MJOen (Fig. 7c). In contrast, for the EDDYc run the MLD deepening is greater than in the other runs, leading a decrease in the BLT by the end of the run (Figs. 7c 12d).

In all runs, SST decreases by 0.25–0.5°C through the run, with NOEDDY simulating the greatest cooling (Figs. 12 and 13a). The SST in the EDDY runs (EDDYa, EDDYb and EDDYc) cooled less than NOEDDY (by 0.02 °C, 0.2 °C and 0.21 °C, respectively) (Fig. 13). Similar to experiment MJOen, the run initialized with the profile with shallowest MLD (run EDDYa) had the greatest cooling, and thus, this experiment is the closest to the NOEDDY run in terms of temperature anomalies (i.e. temperature difference at the end of simulation; Fig. 13a).

The results shows that the similar surface fluxes applied to experiments MJOen and MJOenW led to cooling and freshening of the waters above the ML, and similar deepening of the ILD (Fig. 5). However, the stronger winds used to force experiment MJOenW led to a stronger wind-induced mixing and deepening of the MLD by 10-15 m by the end of these runs (Fig. 12), unlike the experiment MJOen results (Fig. 10). As a consequence, the thickening of the BL during the MJOenW-EDDY runs is smaller than in the MJOen-EDDY EDDY runs. For the MJOenW-NOEDDY run, wind mixing did not allow the formation of the BL, as observed in the MJOen-NOEDDY run, and the water column is thoroughly mixed down to the ILD (30 m; Fig. 12a). As a consequence of this deeper mixing, the cooling experienced by these surface waters in the MJOenW-NOEDDY run was greater than that experienced in experiment MJOen-NOEDDY.

In contrast to the MJOenW-NOEDDY run, for the MJOenW-EDDY runs the BL was initially present and remained for the entire runs, isolating the surface waters and contributing to reduce the intense vertical mixing (Fig. 12). As a result, the cooling experienced by surface waters in the MJOenW-EDDY runs was virtually the same as in MJOen-EDDY runs, despite the stronger winds (Figs. 10b,c,d and 12b,c,d). Consequently, the cooling experienced by surface waters for the MJOenW-EDDY runs, when the BL was present, was smaller than that experienced by waters in MJOenW-NOEDDY run, where BL was absent (Fig. 13).

Even when the MJOenW-NOEDDY and MJOenW-EDDY runs are initialised with profiles of similar stratification strength (ϕ ~ 20 J m^{-3}; runs MJOenW-NOEDDY and MJOenW-EDDYb; Figs. 13a,c), less cooling of ML waters occurs when the BL is present. While the wind-induced mixing was able to fully mix waters down to the ILD when the BL was absent, it was not able to sufficiently erode the preexisting BL, thus leading to less cooling of ML waters by subsurface entrainment. This highlights the role of a preexisting BL (and thus salinity stratification) in modulating the SST response to the atmospheric forcing. Among the EDDY runs, the results suggest that the magnitude of the difference in cooling of those from the NOEDDY run is related to their difference in MLD. This suggests that, once the pre-existing BL is sufficiently thick to counteract the wind-induced mixing, MLD and ML heat capacity will then play a role in determining the magnitude of the SST change. The ocean evolution for the different experiments is summarised in an schematic (Fig. 14).

8. Further Discussions and Conclusions

Using observations from a two-month ocean glider deployment in the southeast Indian Ocean, we demonstrate quantitatively that for the first 20 days, local surface fluxes determined by the suppressed phase were the primary drivers of upper ocean temperature and salinity variability. Ocean dynamics then became an important additional driver with the passage of a fresh-core mesoscale eddy originating from the coast of Java.

Besides the advection of relatively warmer waters within the eddy, which directly affect heat fluxes, the eddy had a secondary potential effect on ocean SST by affecting ocean stratification and thus modulating surface and subsurface heat fluxes. By changing the water column stability, eddy advection led to the development of a BL that lasts longer than the eddy's altimetric signature. Thus, this process has a lasting effect on ocean–atmosphere interaction that has not previously been explicitly considered. These results highlight the capability of gliders to provide critical data to improve our understanding of MJO dynamics, as the vertical resolution of reanalysis data is not sufficiently fine to evaluate changes in ocean stratification in such detail.

Based solely on the effect of the BL on the ML heat capacity through changes in the MLD, we estimate that the eddy-induced BL leads to an extra SST increase of $\approx$ 0.4 °C (10 day)$^{-1}$ during the observed suppressed MJO phase. Our 1-D mixed layer modelling experiments corroborate these findings, showing consistently a greater SST increase when a BL is initially present under a suppressed MJO forcing, regardless of the MLD and BLT structure. In these experiments, not only changes in the ML heat capacity are considered, but also mixing through convective instability, entrainment from the pycnocline, and mixing through enhanced vertical current shear, leading to a final estimate of 0.15-0.25 °C of extra increase in SST after 10 days, if a BL is present. This more accurate estimate is still in the same order of magnitude of our initial estimate of extra SST increase, and within the range of typical MJO-induced SST anomalies (0.2–0.5 °C; DeMott et al., 2015), thus having a physical significance for ocean–atmosphere interaction.

Under typical conditions of a MJO convective (enhanced) phase, the modelling experiments show that the impact of the BL on the cooling of the surface waters depends the relative strength of wind-induced mixing in comparison with the water column stratification. When winds are relatively weak, a BL can develop if initially absent, and an existing BL can thicken. As a result, surface waters are isolated from below, and the magnitude of the cooling will be mostly dependent on the MLD and not necessarily on the BL thickness. Thus, the initial presence of a BL is not necessarily a defining factor of the magnitude of the SST change. However, when winds are sufficiently strong, it is less likely that a BL will develop if initially absent, but an existing BL is likely to persist. In this case, where the BL persists, the cooling of surface waters is less than where the BL is absent. Once the existing BL is able to persist, the magnitude of the temperature change will be mostly dependent on the MLD and the ML heat content, not necessarily on its thickness. Thus, the overall effect of the atmospheric forcing on the SST is dependent on the relationship between the strength of wind forcing and the ocean subsurface structure, including both MLD and BLT. These results highlight the importance of the ocean subsurface precondition in modulating the SST response to the atmospheric forcing, and the need for representing those accurately for appropriate modelling of air-sea interaction in this region. It also suggests that SST can respond differently to different MJO events, as individual events are highly variable.

Based on composited observations, Drushka et al. (2014) estimated that a BLT of 10 m is sufficient to reduce MJO-induced ML temperature anomalies by 0.1–0.2 °C during its enhanced phase, likely due to reduced vertical entrainment. Our modelling estimates are consistent with those findings. Our runs are based on real conditions, i.e., the parameters used to force the model were based on the atmospheric conditions during our observations, while the different profiles used to initialize the model represented the variety of oceanic conditions encountered over a course of three days within a single, observed eddy. These included profiles with ϕ_{40m}, MLD and BLT ranging between 7–44 J.m^{-3}, 10–27 m and 7–18 m, respectively. For those, we estimate SST anomalies between beginning and end of 10-days runs of 0.02–0.21 °C under enhanced MJO forcing, when we compare runs initialized from different profiles with and without a BL, i.e. from inside and outside the eddy. As realistic estimates, such SST anomalies have a physical significance and highlight the meaningful impact that fresh-core eddies potentially have in local air-sea interactions at these time scales.

Therefore, the model experiments forced with enhanced MJO atmospheric conditions support the hypothesis suggested by our glider observations: by inducing a thick BL during the suppressed phase, the eddy-generated near-surface stratified conditions likely allowed the BL to persist and develop during the enhanced precipitation phase, aided by further salinity stratification from precipitation. In doing so, the eddy-induced BL also contributed to the isolation of the surface from the colder and saltier waters below the ML, and as a result, retaining heat within this layer and likely reducing further the MJO-induced cooling. Thus, the presence of a thick eddy-induced BL during the suppressed phase likely modulated the magnitude of temperature anomalies forced by surface fluxes during the following enhanced phase. As a consequence, the timing of periods of enhanced eddy activity relative to the development of MJO events is critical to determine the feedback between them.

Not all SETIO eddies will have a warm-fresh core, and thus only a fraction of it will have the potential to generate a BL. However, eddy generation is frequent in this region, with eddies having an average life span of 50 $\pm$ 22 days (Wang et al., 2021). As such, these eddies, and consequently their local effect on the upper ocean, can last for longer than the eddy sampled here. Therefore, we anticipate that during highly energetic periods these features will likely have an important impact on coupled ocean–atmosphere systems such as the MJO.

Ocean mesoscale processes are not typically included in climate model runs of the MJO (e.g., DeMott et al., 2015). Our study suggests that, to capture MJO-related SST variability accurately, such models should take into account the secondary effects on SST induced by fresh-core eddies through changing ocean stratification, and the timing between enhanced eddy activity relative to the evolution of the atmospheric weather system. Therefore, we argue that mesoscale ocean dynamics is potentially a missing ingredient in MJO forecasting. Recent developments in operational weather forecasting with eddy-resolving ocean models coupled to high-resolution atmospheric models (e.g. at the UK Met Office; Williams, Copsey, Blockley, BodasâĂŘSalcedo, Calvert, Comer, Davis, Graham, Hewitt, Hill, Hyder, Ineson, Johns, Keen, Lee, Megann, Milton, Rae, Roberts, Scaife, Schiemann, Storkey, Thorpe, Watterson, Walters, West, Wood, Woollings and Xavier, 2018) will likely allow a more comprehensive assessment of the role of mesoscale ocean dynamics within the MJO.

9. Open Research

The glider data used in the study are available at the British Oceanographic Data Centre (BODC) via https://www.bodc.ac.uk/data/published_data_library/catalogue/10.5285/efcc09dc-ed05-775c-e053-6c86abc0bb49/.

10. Acknowledgments

This work was part of the Equatorial Line Observations project, funded by the UK Natural Environment Research Council (NERC; grant NE/R012431/1) and the US National Science Foundation (NSF; grant 1724741), and the TerraMaris project (NERC; grant NE/R016704/1). D.B.B. was supported by the Poland's National Science Center (NCN;project no. 2022/45/B/ST10/03836).

11. Tables and Figures

Table 1
Experiments run using PWP model and the periods used to produce the forcing in each case. Each period represents different MJO conditions experienced during the glider deployment: MJOsup - suppressed convection phase, MJOen - enhanced convection phase and MJOenW enhanced convection phase with stronger winds.

Experiments	**Forcing**
MJOsup	2019-02-10 to 2019-02-20
MJOen	2019-03-03 to 2019-03-13
MJOenW	2019-01-18 to 2019-01-28 (wind stress and latent heat flux) 2019-03-03 to 2019-03-13 (remaining variables)

Table 2
Mixed layer depth (MLD), barrier layer thickness (BLT) and potential energy anomaly integrated from the surface to a depth (H) of 40 m (ϕ_{40}) for each profile used to initialise the different runs (NOEDDY, EDDYa, EDDYb and EDDYc) for each experiment (see Table 1).

Runs	**NOEDDY**	**EDDYa**	**EDDYb**	**EDDYc**
Profile day (mm-dd)	02-13	02-19	02-20	02-21
MLD (m)	25	10	15	27
BLT (m)	0	7	18	10
ϕ_{40} (J m^{-3})	19.3	44	21	6.8

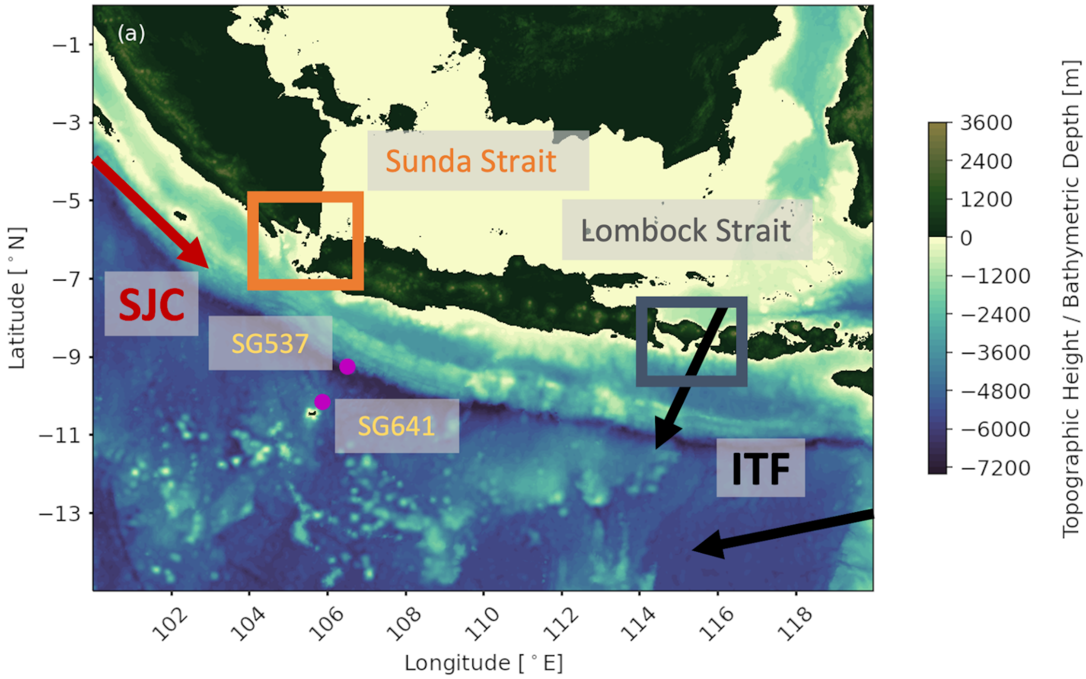

Figure 1: GEBCO bathymetry (m) with locations of gliders SG537 (106 °32′ E, 9 °15′ S) and SG641 (105 °54′ E, 10 °10′ S) (pink dots). Red and black arrows show South Java Current (SJC) and Indonesian Through Flow (ITF) pathways, respectively.

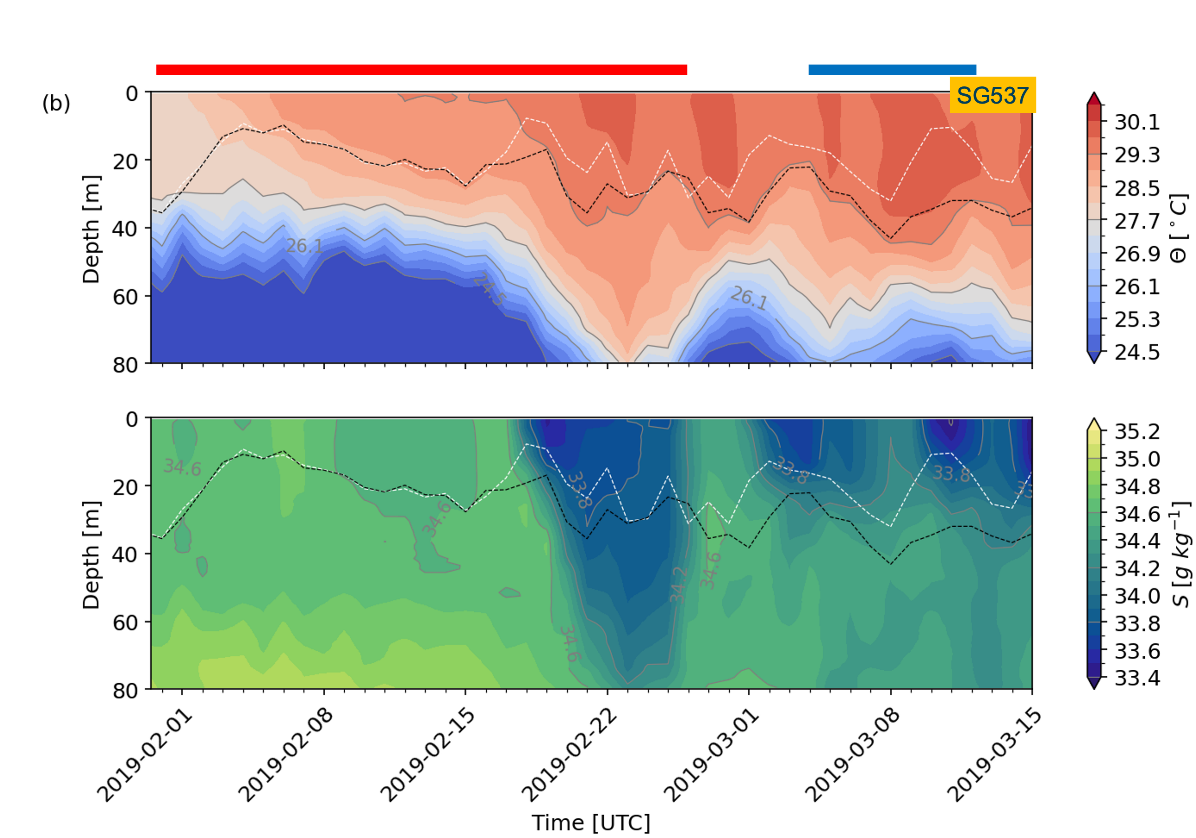

Figure 2: Daily average conservative temperature (Θ) and absolute salinity (S) from glider SG537. White and black dotted contours show daily-averaged MLD and ILD, respectively. Red and blue horizontal bars indicate suppressed and enhanced MJO phases.

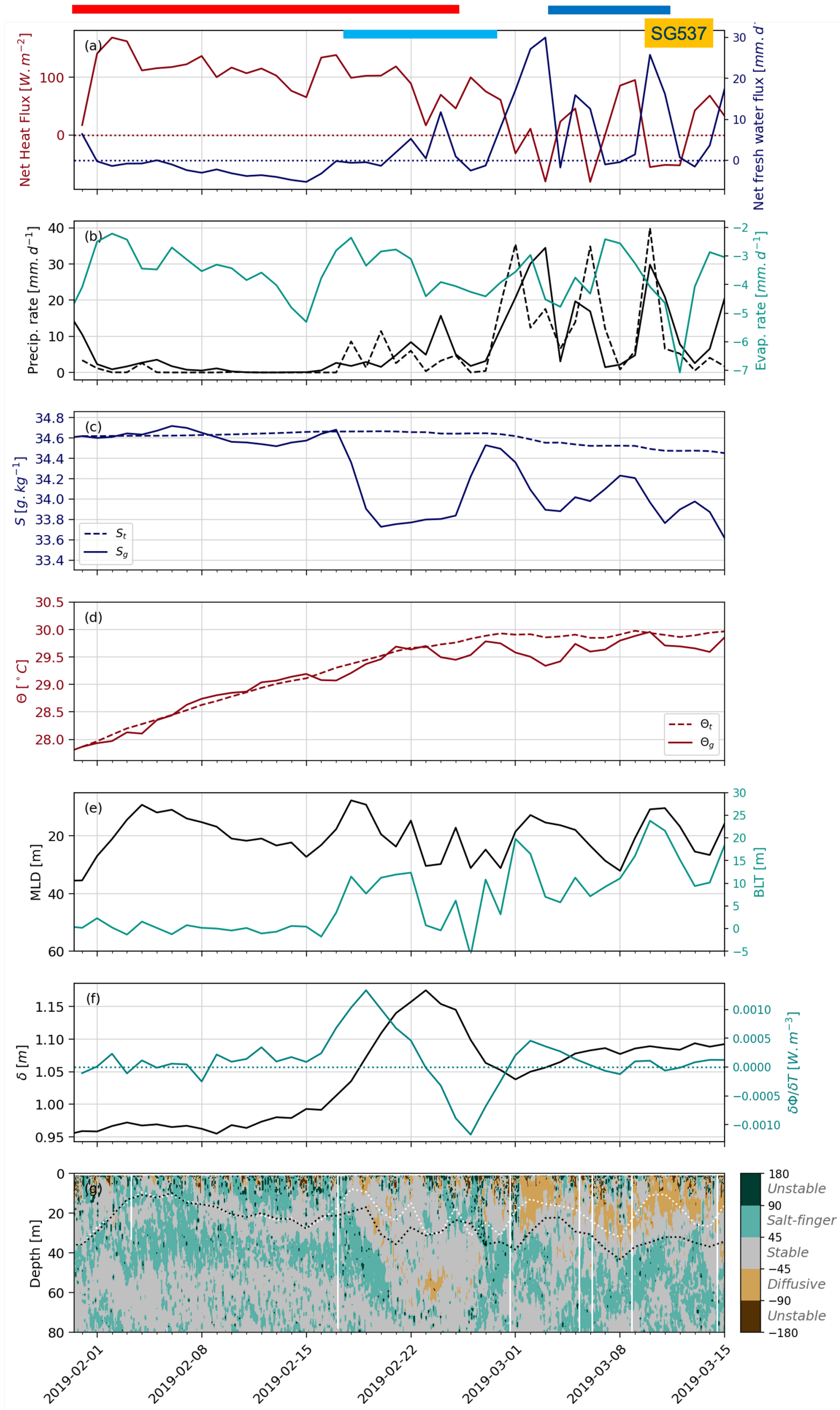

Figure 3: Daily average time series at the location of glider SG537. (a) Net surface heat flux (positive downward; brown) and net freshwater flux (dark blue) from ERA5 (averaged over a 1 ° box at the glider location). (b) Precipitation (black) and evaporation (green) from ERA5, and precipitation from TRMM 3B42 (dotted black). Panels (c) and (d) show theoretical (dotted line) and observed (full line) absolute salinity (S_t and S_g) and conservative temperature (Θ_t and Θ_g), respectively. (e) Mixed layer depth (MLD; black) and barrier layer thickness (BLT; green). (f) Steric height anomaly (δ; black) and potential energy anomaly tendency ($\partial\phi/\partial t$; green) from the glider. (g) Turner angle (degrees). Light blue bar indicates eddy sampling period. Red and dark blue bars as in Fig. 2.

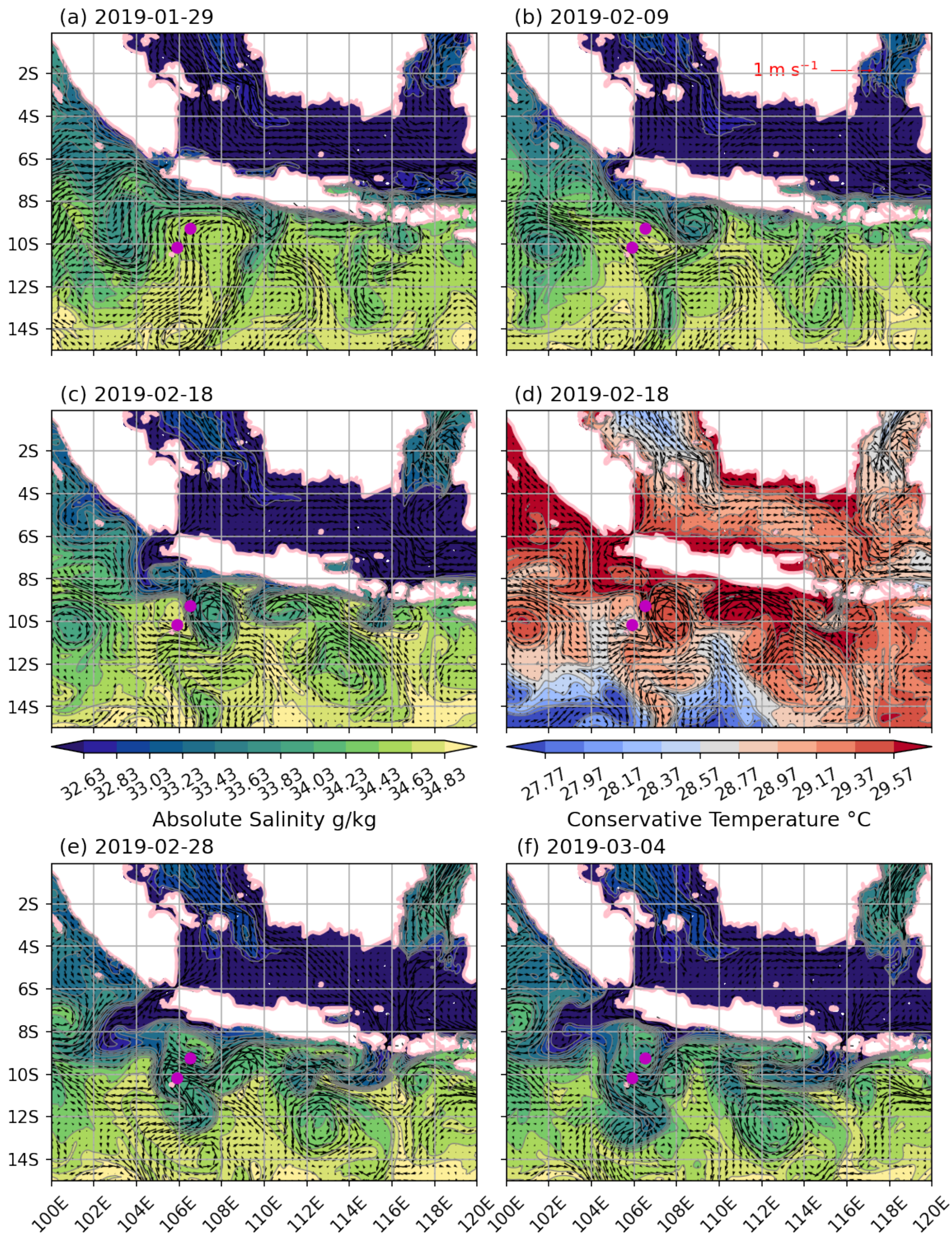

Figure 4: Surface layer (0–25 m average) daily snapshots of absolute salinity (panels a, b, c, e and f), conservative temperature (panel d) and surface currents (arrows) from GLORYS12V1. Glider locations are indicated by pink dots.

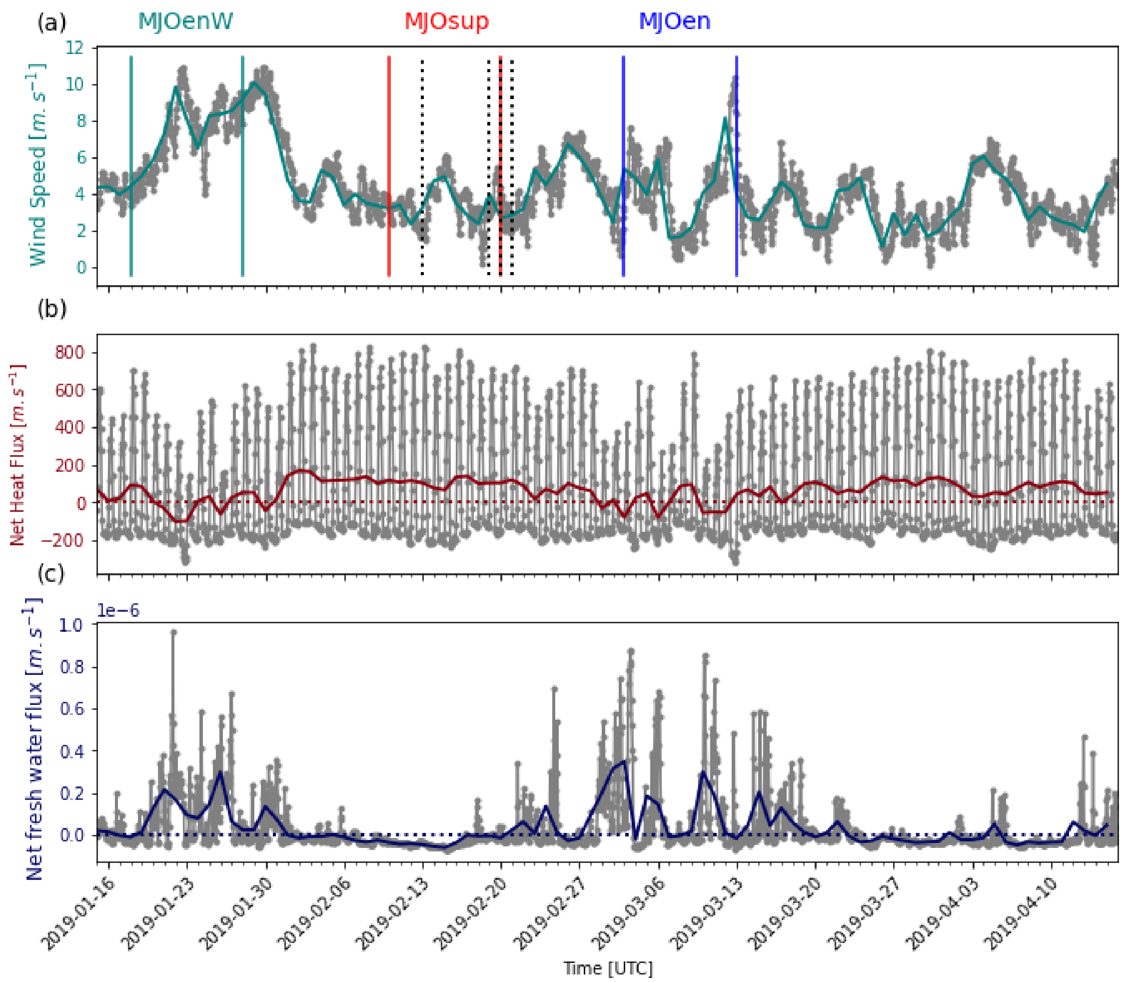

Figure 5: Daily average time series of atmospheric forcing at the location of glider SG537. (a) Wind Speed, (b) net surface heat flux (positive downward; brown) and (c) net freshwater flux (dark blue) from ERA5 (averaged over a 1 ° box at the glider location). Grey lines show daily time series. Vertical lines indicate days of profiles chosen for runs (dotted black) and periods used to produce forcing for the experiments MJOsup (red), MJOen (blue) and MJOenW (green).

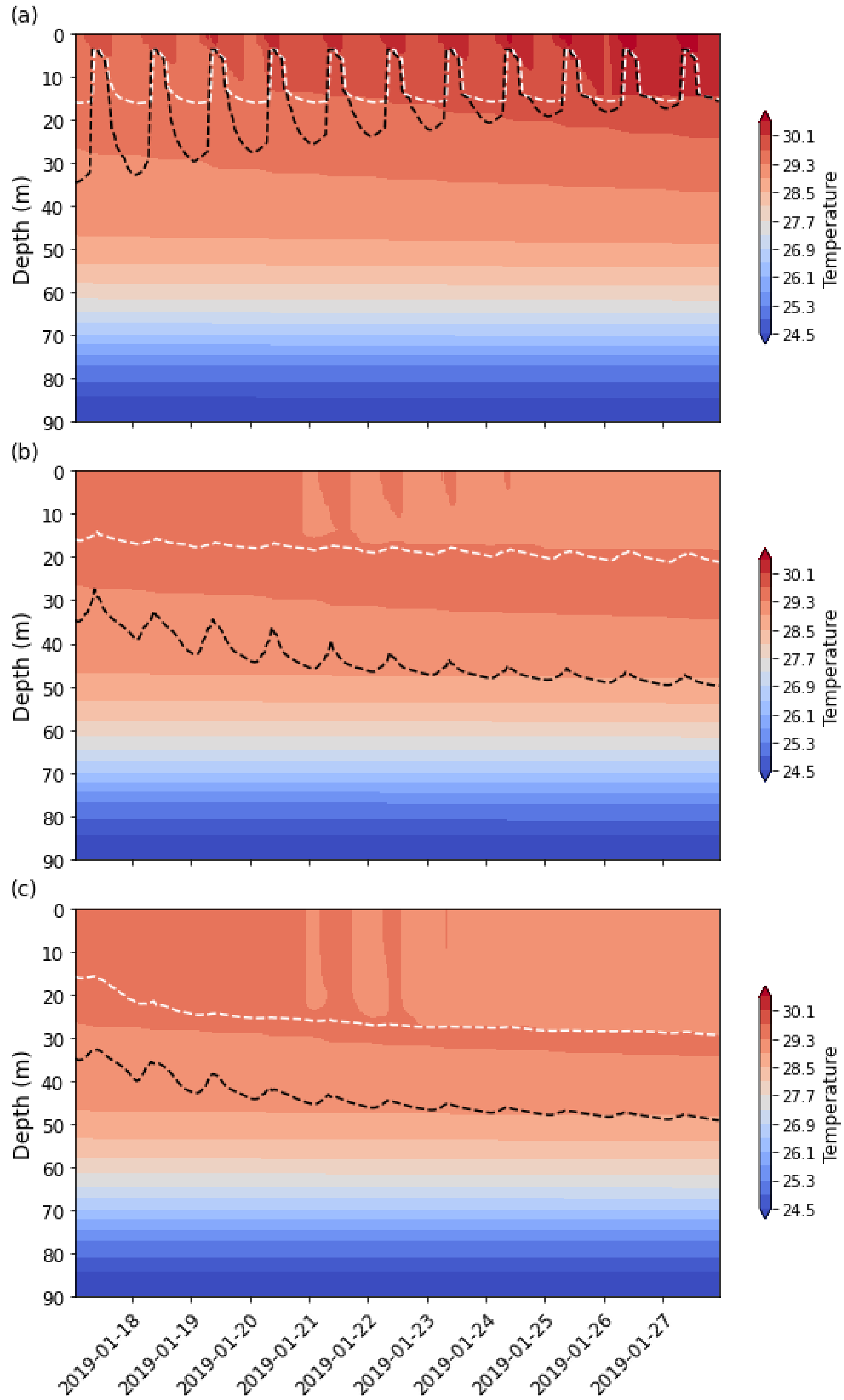

Figure 6: Temperature from model hourly output for (a) Experiment MJOsup-EDDYb, (b) MJOen-EDDYb and (c) MJOenW-EDDYb (initial conditions from 20-02-2019). Dashed white and black lines represent MLD and ILD respectively.

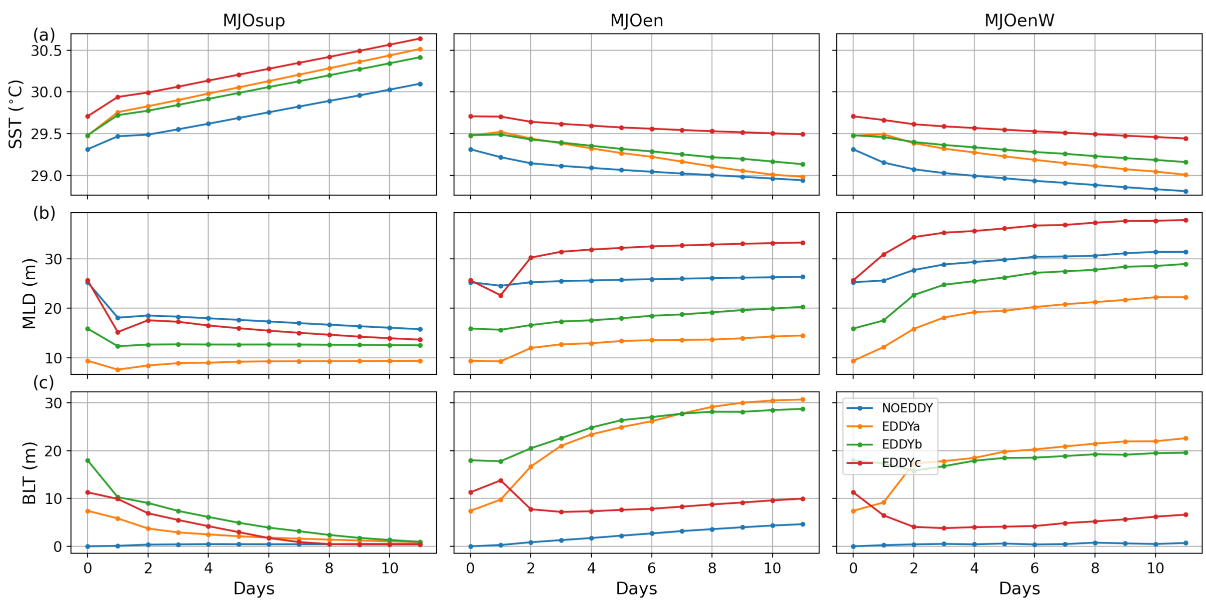

Figure 7: Daily average time series of (a) SST, (b) MLD and (c) BLT from experiments MJOsup (left), MJOen (middle) and MJOenW (right). Data points at day 0 indicates values from profile used to initialize the run. Colours corresponding to each run are shown in legend.

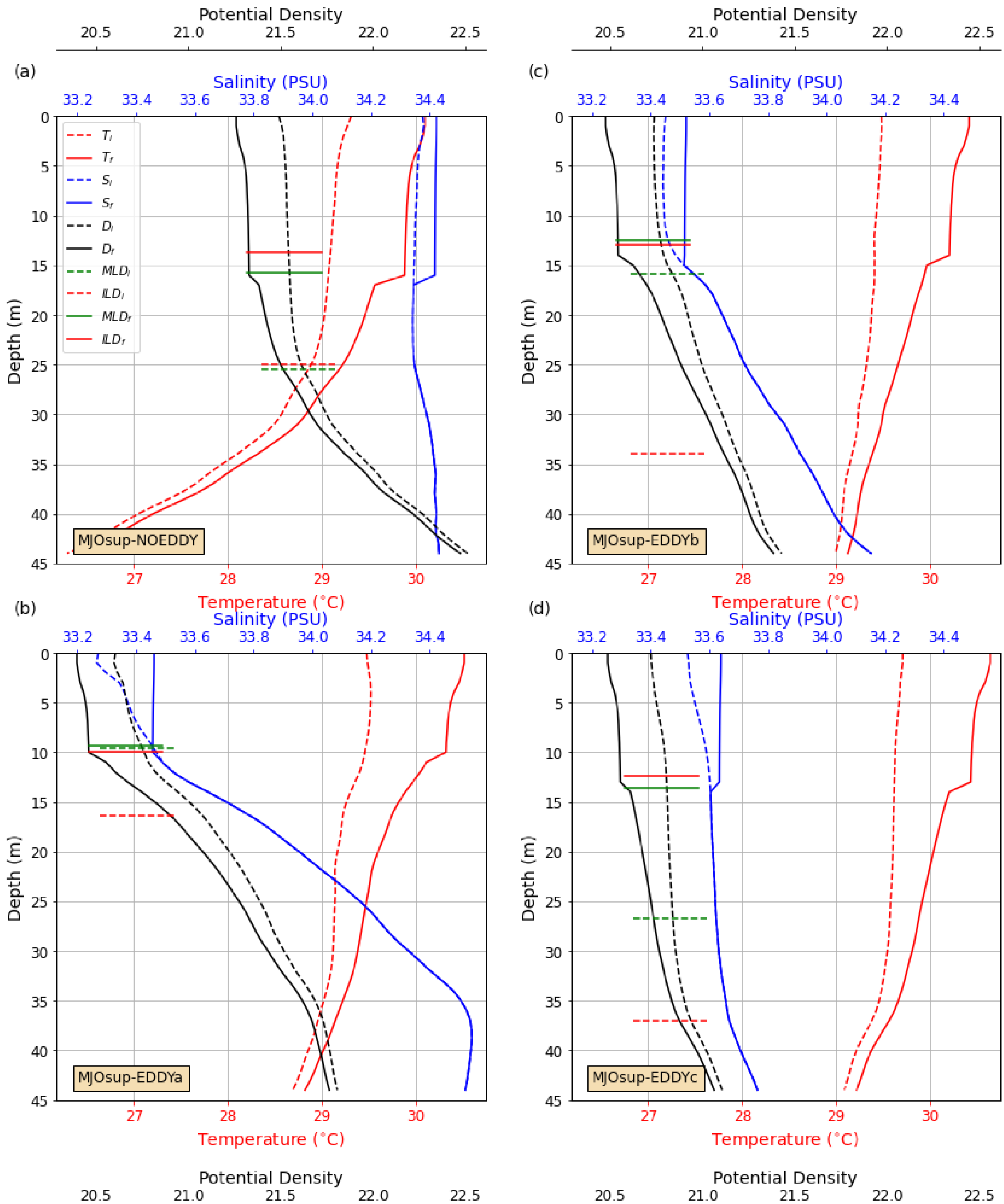

Figure 8: Experiment MJOsup: Comparison of initial profiles (dashed lines) and final profiles (full lines) from the model for runs (a) MJOsup-NOEDDY; (b) MJOsup-EDDYa,(c) MJOsup-EDDYb, and (d) MJOsup-EDDYc. Temperature (° C), salinity and potential density (kg m $^{-3}$) are shown in red, blue and black, respectively. Horizontal red and green lines indicate MLD and ILD for initial profiles (dashed lines) and final model output (full lines).

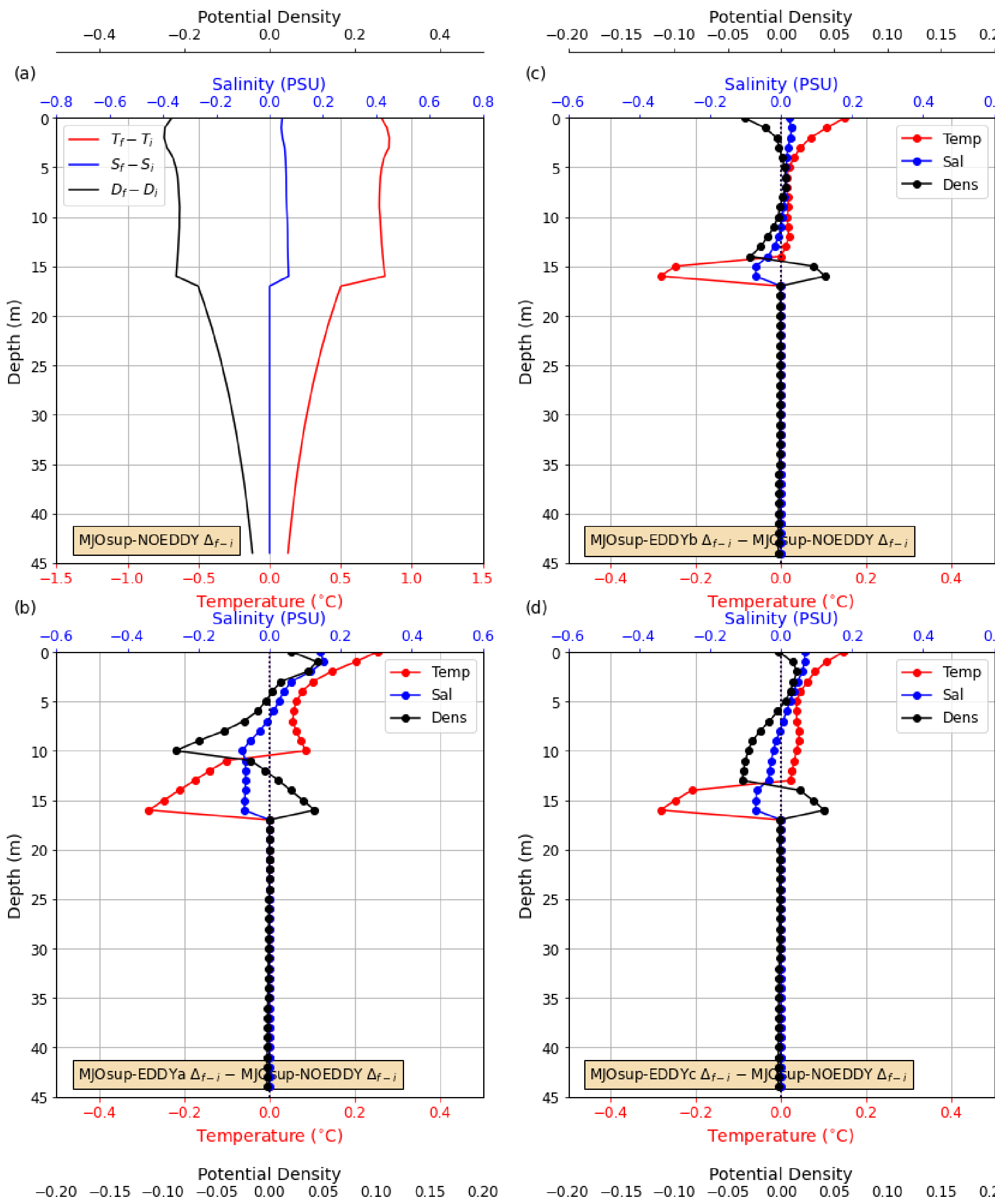

Figure 9: Experiment MJOsup: (a) Anomalies (i.e. differences at the end of simulation; Δ_{f-I}) from model run MJOsup-NOEDDY. Difference between anomalies from the model run MJOsup-NOEDDY (shown in panel a) and anomalies from model runs (b) MJOsup-EDDYa, (c) MJOsup-EDDYb and (c) MJOsup-EDDYc; (MJOsup-EDDY Δ_{f-I} − MJOsup-NOEDDY Δ_{f-I}). Temperature (° C), salinity and potential density (kg m^{-3}) differences are shown in red, blue and black, respectively

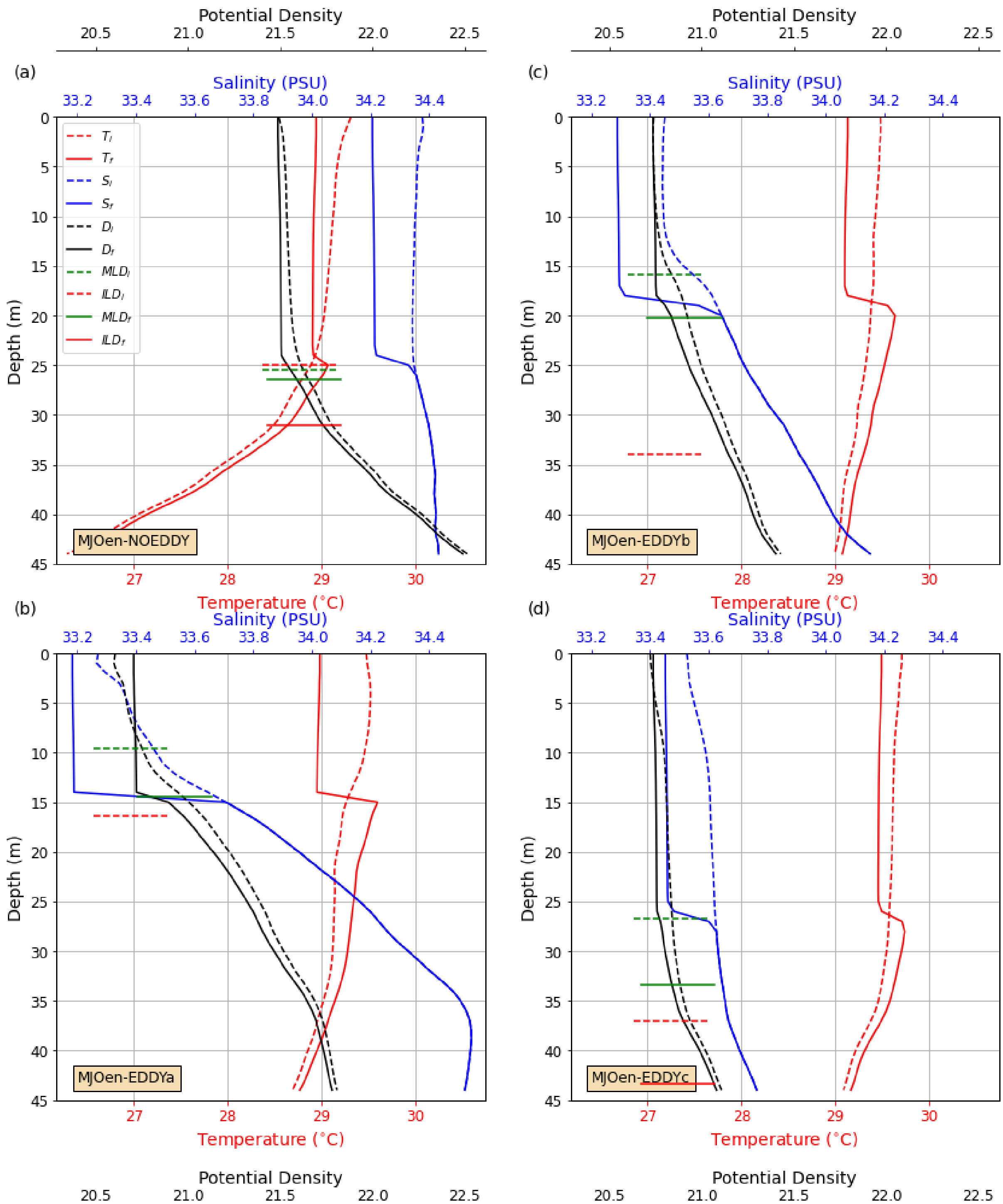

Figure 10: As in figure 8, but for experiment MJOen.

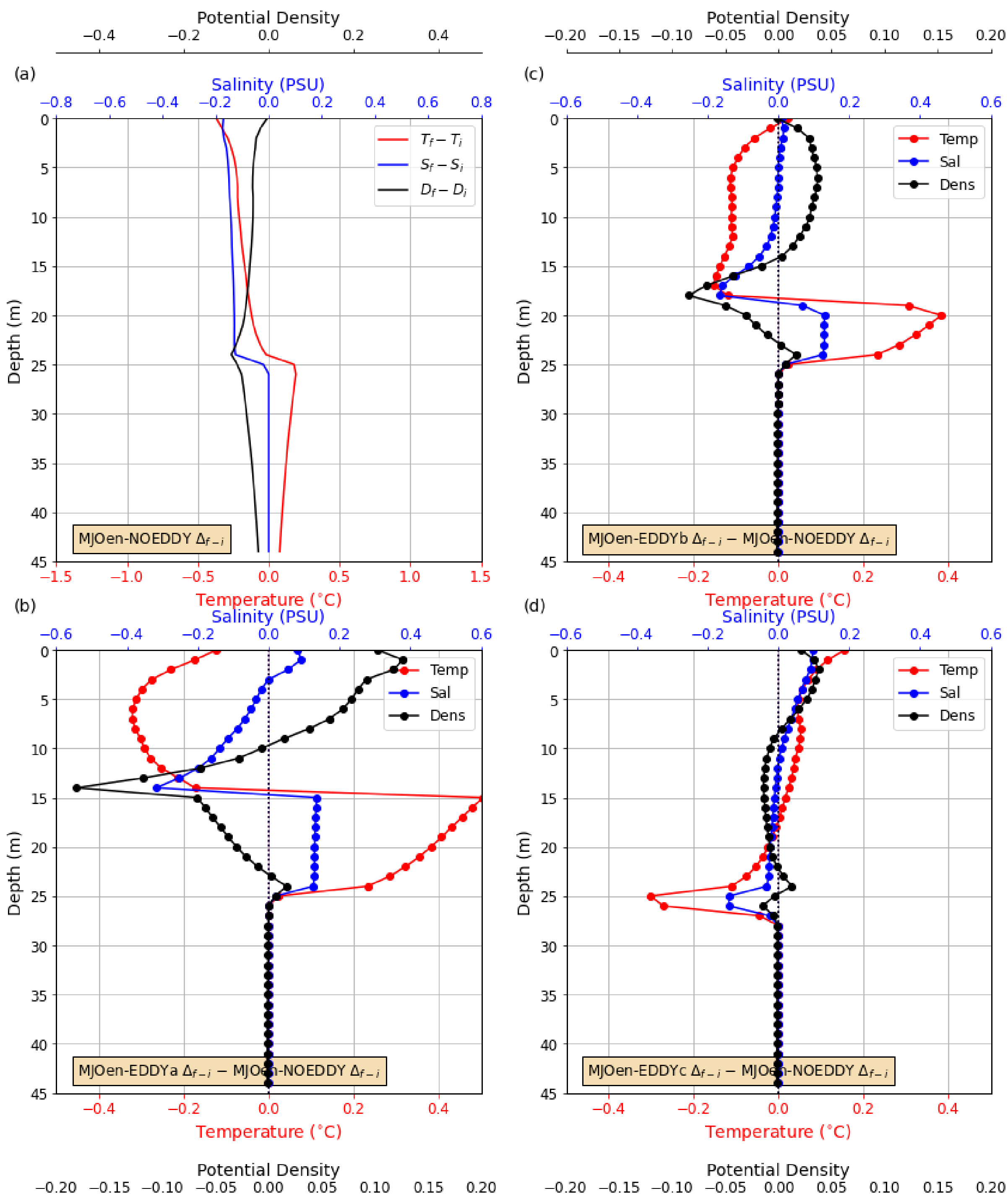

Figure 11: As in figure 9, but for experiment MJOen

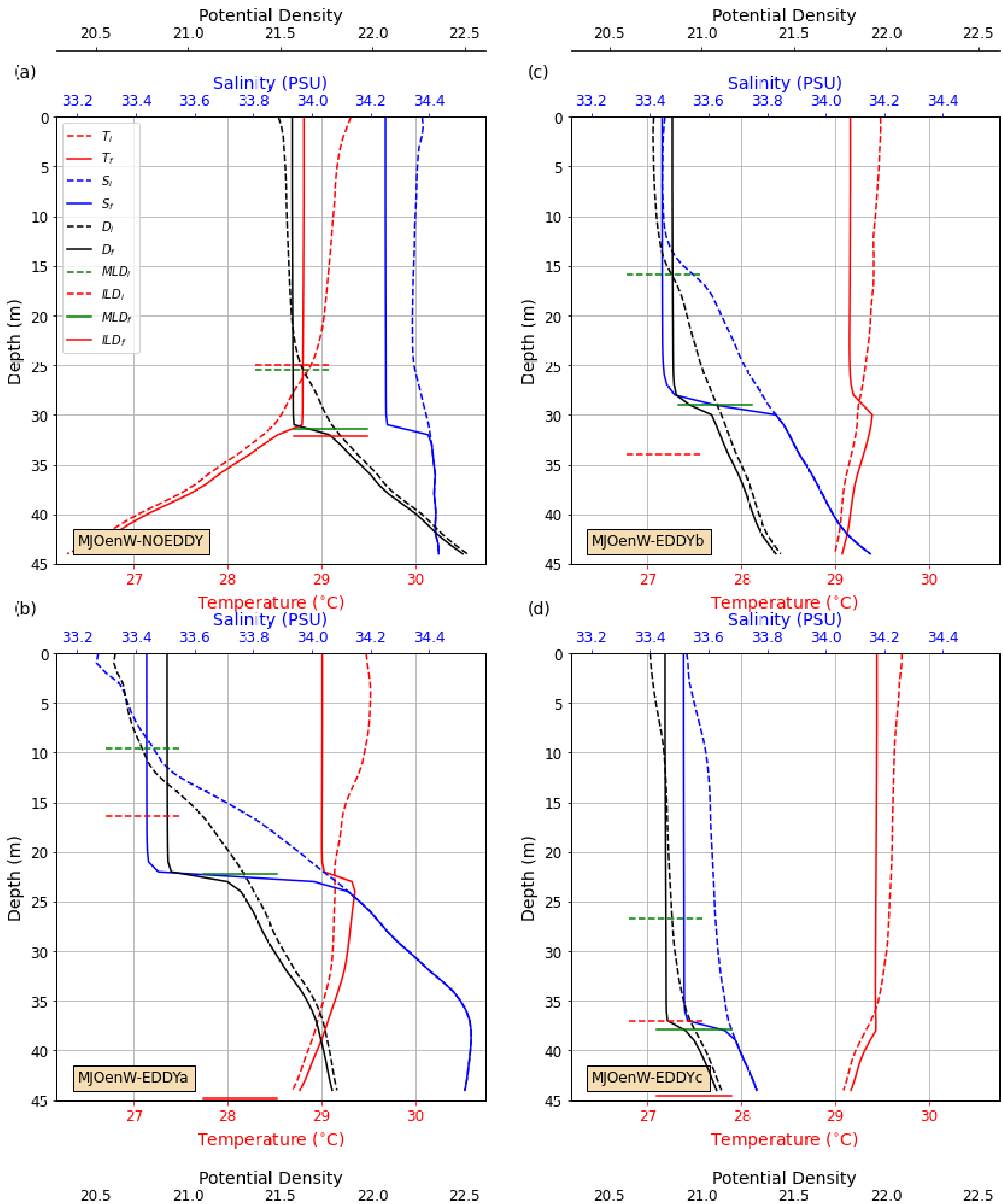

Figure 12: As in figure 8, but for experiment MJOenW.

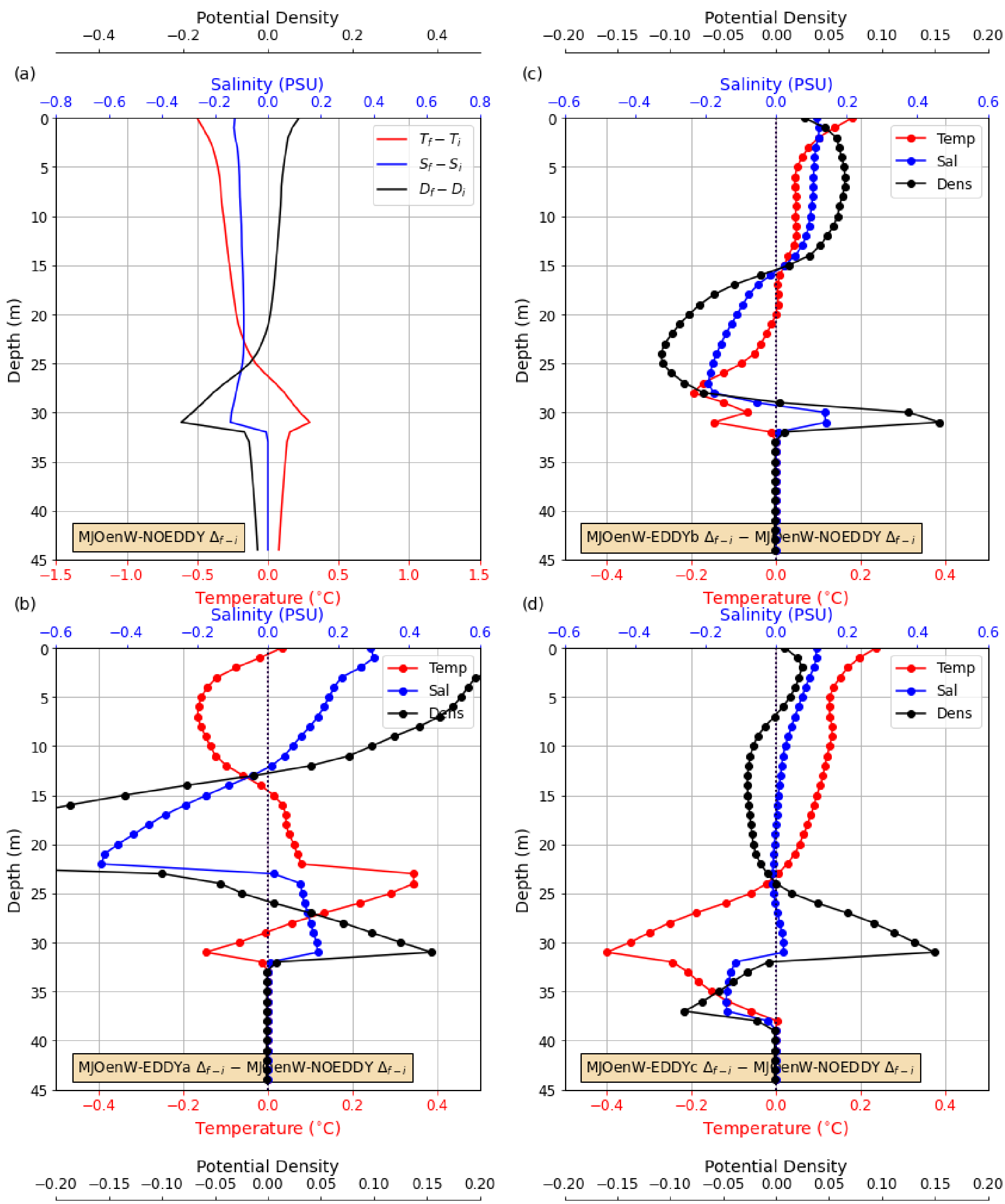

Figure 13: As in figure 9, but for experiment MJOenW

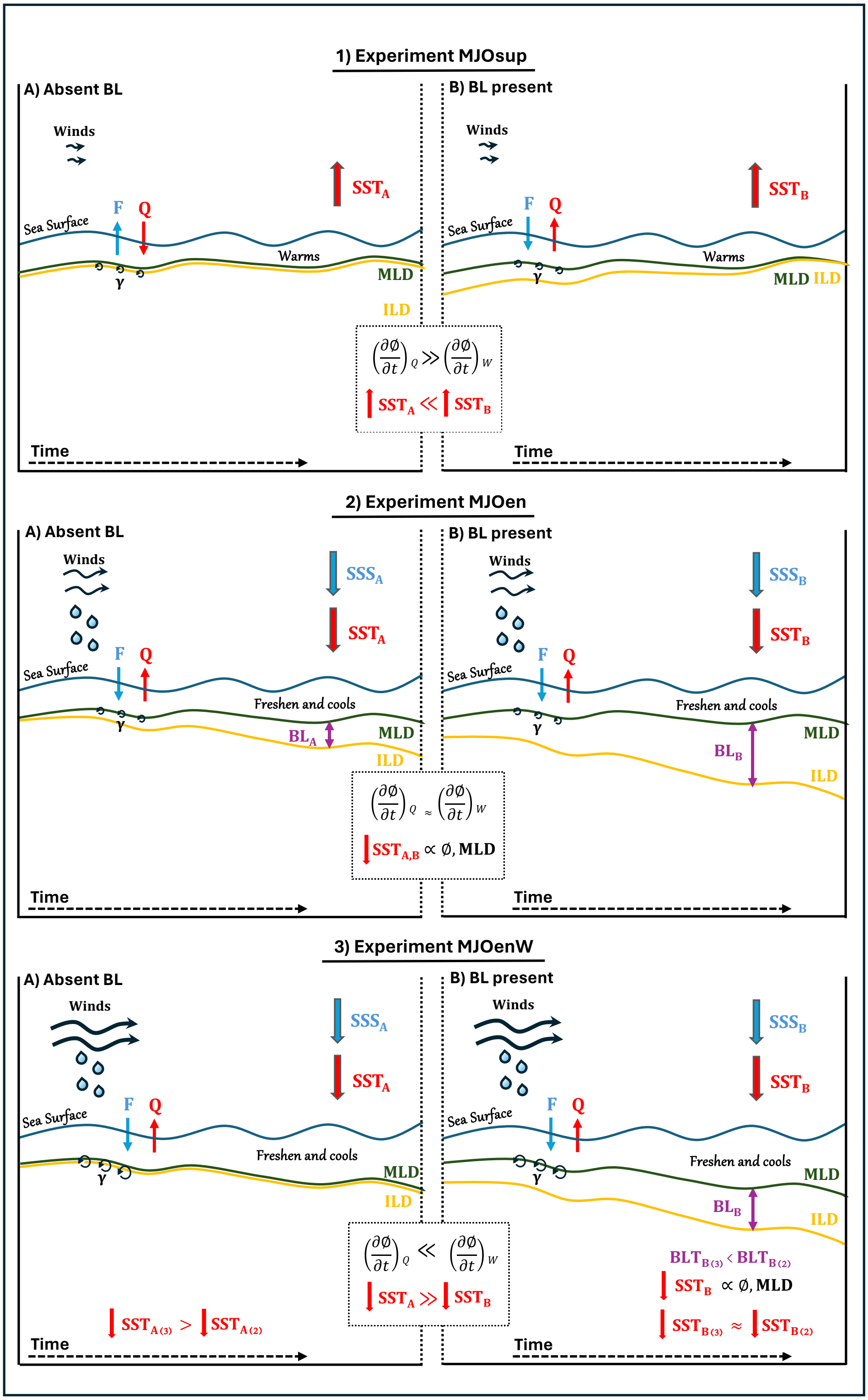

Figure 14: Schematic showing the general evolution of oceanic conditions under the modeling experiments (1) MJOsup, (2) MJOen and (3) MJOenW. Panels (A) represent initial conditions where the BL was initially absent (run NOEDDY) and (B) where it was present (runs EDDYa, EDDYb and EDDYc). The difference in wind stress between experiments is shown by the size of the wavy arrows, while precipitation is indicated by the water drops. Blue and red arrows at ocean surface represent the direction of the heat (Q) and fresh water (F) surface fluxes. Changes in sea surface temperature (SST) and sea surface salinity (SSS) through the experiment are indicated by the adjacent arrows. Purple arrow indicates the thickness of the barrier layer (BL). Turbulent mixing at the base of the mixed layer also varies between experiments and is represented by γ. The relative contribution of heat fluxes and wind mixing to changes in stratification $(\partial\phi/\partial t)$ is shown in the inserted box for each experiment. The increase in barrier layer thickness shown in panels 2b and 3b are only representative of runs EDDYa and EDDYb, but not EDDYc (see sections 7.3 and 7.4 for more details).

References

Alford, M.H., 2020. Revisiting near-inertial wind work: Slab models, relative stress, and mixed layer deepening. Journal of Physical Oceanography 50, 3141–3156. doi:10.1175/JPO-D-20-0105.1.

Balaguru, K., Foltz, G.R., Ruby Leung, L., Kaplan, J., Xu, W., Reul, N., Chapron, B., 2020. Pronounced impact of salinity on rapidly intensifying tropical cyclones. Bulletin of the American Meteorological Society 101, E1497–E1511. doi:10.1175/BAMS-D-19-0303.1.

Baranowski, D.B., Flatau, P.J., Chen, S., Black, P.G., 2014. Upper ocean response to the passage of two sequential typhoons. Ocean Science 10, 559–570. doi:10.5194/os-10-559-2014.

Bray, N.A., Wijffels, S.E., Chong, J.C., Fieux, M., Hautala, S., Meyers, G., Morawitz, W.M., 1997. Characteristics of the Indo-Pacific throughflow in the eastern Indian Ocean. Geophysical Research Letters 24, 2569–2572. doi:10.1029/97GL51793.

Cassou, C., 2008. Intraseasonal interaction between the Madden-Julian Oscillation and the North Atlantic Oscillation. Nature 455, 523–527. doi:10.1038/nature07286.

Da Silva, N.A., Matthews, A.J., 2021. Impact of the MaddenâĂŞJulian Oscillation on extreme precipitation over the western Maritime Continent and Southeast Asia. Quarterly Journal of the Royal Meteorological Society 147, 3434–3453. doi:10.1002/qj.4136.

Damerell, G.M., Heywood, K.J., Calvert, D., Grant, A.L., Bell, M.J., Belcher, S.E., 2020. A comparison of five surface mixed layer models with a year of observations in the North Atlantic. Progress in Oceanography 187, 102316. doi:10.1016/j.pocean.2020.102316.

Damerell, G.M., Heywood, K.J., Thompson, A.F., Binetti, U., Kaiser, J., 2016. The vertical structure of upper ocean variability at the Porcupine Abyssal Plain during 2012âĂŞ2013. Journal of Geophysical Research: Oceans 121, 3075–3089. doi:10.1002/2015JC011423.

DeMott, C.A., Benedict, J.J., Klingaman, N.P., Woolnough, S.J., Randall, D.A., 2016. Diagnosing ocean feedbacks to the MJO: SST-modulated surface fluxes and the moist static energy budget. Journal of Geophysical Research 121, 8350–8373. doi:10.1002/2016JD025098.

DeMott, C.A., Klingaman, N.P., Woolnough, S.J., 2015. Atmosphere-ocean coupled processes in the Madden-Julian oscillation. Reviews of Geophysics 53, 1099–1154. doi:10.1002/2014RG000478, arXiv:arXiv:1011.1669v3.

Drushka, K., Sprintall, J., Gille, S.T., 2014. Subseasonal variations in salinity and barrier-layer thickness in the eastern equatorial Indian Ocean. Journal of Geophysical Research: Oceans 119, 805–823. doi:10.1002/2013JC009422.

Feng, M., Wijffels, S., 2002. Intraseasonal variability in the South Equatorial Current of the East Indian Ocean. Journal of Physical Oceanography 32, 265–277. doi:10.1175/1520-0485(2002)032<0265:IVITSE>2.0.CO;2.

Gadgil, S., Joseph, P.V., Joshi, N.V., 1984. Ocean-atmosphere coupling over monsoon regions. Nature 312, 141–143. doi:10.1038/312141a0.

Godfrey, J.S., Lindstrom, E.J., 1989. The heat budget of the equatorial western Pacific surface mixed layer. Journal of Geophysical Research 94, 8007. doi:10.1029/jc094ic06p08007.

Hersbach, H., Bell, B., Berrisford, P., Hirahara, S., Horányi, A., Muñoz-Sabater, J., Nicolas, J., Peubey, C., Radu, R., Schepers, D., Simmons, A., Soci, C., Abdalla, S., Abellan, X., Balsamo, G., Bechtold, P., Biavati, G., Bidlot, J., Bonavita, M., De Chiara, G., Dahlgren, P., Dee, D., Diamantakis, M., Dragani, R., Flemming, J., Forbes, R., Fuentes, M., Geer, A., Haimberger, L., Healy, S., Hogan, R.J., Holm, 2020. The ERA5 global reanalysis. Quarterly Journal of the Royal Meteorological Society 146, 1999–2049. doi:10.1002/qj.3803.

IOC, SCOR, IAPSO, 2010. The international thermodynamic equation of seawater âĂŞ 2010: Calculation and use of thermodynamic properties, in: Intergovernmental Oceanographic Commission, Manuals and Guides No. 56, UNESCO, p. 196 pp.

Jiang, X., Adames, Á.F., Kim, D., Maloney, E.D., Lin, H., Kim, H., Zhang, C., DeMott, C.A., Klingaman, N.P., 2020. Fifty Years of Research on the Madden-Julian Oscillation: Recent Progress, Challenges, and Perspectives. Journal of Geophysical Research: Atmospheres 125, 1–64. doi:10.1029/2019JD030911.

Kummerow, C., Simpson, J., Thiele, O., Barnes, W., Chang, A.T.C., Stocker, E., Adler, R.F., Hou, A., Kakar, R., Wentz, F., Ashcroft, P., Kozu, T., Hong, Y., Okamoto, K., Iguchi, T., Kuroiwa, H., Im, E., Haddad, Z., Huffman, G., Ferrier, B., Olson, W.S., Zipser, E., Smith, E.A., Wilheit, T.T., North, G., Krishnamurti, T., Nakamura, K., 2000. The Status of the Tropical Rainfall Measuring Mission (TRMM) after Two Years in Orbit. Journal of Applied Meteorology 39, 1965–1982. doi:10.1175/1520-0450(2001)040<1965:TSOTTR>2.0.CO;2.

Lellouche, J.M., Eric, G., Romain, B.B., Gilles, G., Angélique, M., Marie, D., Clément, B., Mathieu, H., Olivier, L.G., Charly, R., Tony, C., Charles-Emmanuel, T., Florent, G., Giovanni, R., Mounir, B., Yann, D., Pierre-Yves, L.T., 2021. The Copernicus Global 1/12Âř Oceanic and Sea Ice GLORYS12 Reanalysis. Frontiers in Earth Science 9, 1–27. doi:10.3389/feart.2021.698876.

Li, Y., Wang, F., 2015. Thermocline spiciness variations in the tropical Indian Ocean observed during 2003-2014. Deep-Sea Research Part I: Oceanographic Research Papers 97, 52–66. doi:10.1016/j.dsr.2014.12.004.

Lin, H., Brunet, G., Fontecilla, J.S., 2010. Impact of the Madden-Julian Oscillation on the intraseasonal forecast skill of the North Atlantic Oscillation. Geophysical Research Letters 37, 3–6. doi:10.1029/2010GL044315.

Maes, C., Picaut, J., Belamari, S., 2005. Importance of the salinity barrier layer for the buildup of El Niño. Journal of Climate 18, 104–118. doi:10.1175/JCLI-3214.1.

Plueddemann, A.J., Farrar, J.T., 2006. Observations and models of the energy flux from the wind to mixed-layer inertial currents. Deep-Sea Research Part II: Topical Studies in Oceanography 53, 5–30. doi:10.1016/j.dsr2.2005.10.017.

Price, J.F., Weller, R.A., Pinkel, R., 1986. Diurnal Cycling: observations and models of the upper ocean response to diurnal heating, cooling, and wind mixing. 91, 8411–8427. doi:10.1029/jc091ic07p08411.

Ruddick, B., 1983. A practical indicator of the stability of the water column to double-diffusive activity. Deep Sea Research Part A, Oceanographic Research Papers 30, 1105–1107. doi:10.1016/0198-0149(83)90063-8.

Shinoda, T., Hendon, H.H., Glick, J., 1998. Intraseasonal Variability of Surface Fluxes and Sea Surface Temperature in the Tropical Western Pacific and Indian Oceans. Journal of Climate 11, 1685–1702. doi:10.1175/1520-0442(1998)011<1685:IVOSFA>2.0.CO;2.

Simpson, J.H., Sharples, J., 2012. Seasonal stratification and the spring bloom, in: Introduction to the Physical and Biological Oceanography of Shelf Seas. Cambridge University Press. chapter 12, pp. 173–204. doi:10.1017/CBO9781139034098.009.

Sprintall, J., Tomczak, M., 1992. Evidence of the Barrier Layer in the Surface Layer of the Tropics. Journal Of Geophysical Research 97, 7305–7316.

Vialard, J., Delecluse, P., 1998. An OGCM study for the TOGA decade. Part I: Role of salinity in the physics of the western Pacific fresh pool. Journal of Physical Oceanography 28, 1071–1088. doi:10.1175/1520-0485(1998)028<1071:AOSFTT>2.0.CO;2.

Wang, X., Cheng, X., Liu, X., Chen, D., 2021. Dynamics of Eddy Generation in the Southeast Tropical Indian Ocean. Journal of Geophysical Research: Oceans 126, 1–14. doi:10.1029/2020JC016858.

Webber, B.G.M., Matthews, A.J., Heywood, K.J., 2010. A dynamical ocean feedback mechanism for the Madden-Julian Oscillation. Quarterly Journal of the Royal Meteorological Society 136, 740–754. doi:10.1002/qj.604.

Wheeler, M.C., Hendon, H.H., 2004. An All-Season Real-Time Multivariate MJO Index: Development of an Index for Monitoring and Prediction. Monthly Weather Review 132, 1917–1932. doi:10.1175/1520-0493(2004)132<1917:AARMMI>2.0.CO;2, arXiv:arXiv:1011.1669v3.

Williams, K.D., Copsey, D., Blockley, E.W., BodasâĂŘSalcedo, A., Calvert, D., Comer, R., Davis, P., Graham, T., Hewitt, H.T., Hill, R., Hyder, P., Ineson, S., Johns, T.C., Keen, A.B., Lee, R.W., Megann, A., Milton, S.F., Rae, J.G.L., Roberts, M.J., Scaife, A.A., Schiemann, R., Storkey, D., Thorpe, L., Watterson, I.G., Walters, D.N., West, A., Wood, R.A., Woollings, T., Xavier, P.K., 2018. The Met Office Global Coupled Model 3.0 and 3.1 (GC3.0 and GC3.1) Configurations. Journal of Advances in Modeling Earth Systems 10, 357–380. doi:10.1002/

2017MS001115.
Yang, G., Yu, W., Yuan, Y., Zhao, X., Wang, F., Chen, G., Liu, L., Duan, Y., 2015. Characteristics, vertical structures, and heat/salt transports of mesoscale eddies in the southeastern tropical Indian Ocean. Journal of Geophysical Research: Oceans 120, 6733–6750. doi:10.1002/2015JC011130.
Zhang, C., 2005. Madden-Julian Oscillation. Reviews of Geophysics 43, 1–36. doi:10.1029/2004RG000158.
Zhu, J., Huang, B., Zhang, R.H., Hu, Z.Z., Kumar, A., Balmaseda, M.A., Marx, L., Kinter, J.L., 2014. Salinity anomaly as a trigger for ENSO events. Scientific Reports 4, 1–5. doi:10.1038/srep06821.
Zhu, J., Kumar, A., 2019. Role of sea surface salinity feedback in MJO predictability: A study with CFSv2. Journal of Climate 32, 5745–5759. doi:10.1175/JCLI-D-18-0755.1.

Declaration of interests

☒ The authors declare that they have no known competing financial interests or personal relationships that could have appeared to influence the work reported in this paper.

☐ The authors declare the following financial interests/personal relationships which may be considered as potential competing interests: